atmosphere

MDPI

Article

Southern Hemisphere Shallow Extratropical Cyclones: A 2000–2023 Comprehensive Analysis Using Multi-Level Detection and Tracking

Susan G. Lakkis [1,2,*], Pablo O. Canziani [1,3], Guillermo A. Frank [1] and Adrián E. Yuchechen [1,3]

[1] Unidad de Investigación y Desarrollo de las Ingenierías, Facultad Regional Buenos Aires, Universidad Tecnológica Nacional, Mozart 2300, Buenos Aires C1407IVT, Argentina; pocanziani@frba.utn.edu.ar (P.O.C.); gfrank@frba.utn.edu.ar (G.A.F.); aeyuchechen@frba.utn.edu.ar (A.E.Y.)
[2] Facultad de Ingeniería y Ciencias Agrarias, Pontificia Universidad Católica Argentina, Av. Alicia Moreau de Justo 1500, Buenos Aires C1107AFD, Argentina
[3] Consejo Nacional de Investigaciones Científicas y Técnicas, Buenos Aires C1425FQB, Argentina
* Correspondence: gabylakkis@uca.edu.ar

Abstract

Extratropical cyclones (ETCs) are primary drivers of mid-latitude weather variability, yet most climatologies rely on single-level tracking, leaving their vertical structure poorly characterised. Because the vertical extent of a cyclone reflects its degree of baroclinic coupling and the tropospheric layer in which it resides is closely linked to the dominant physical processes governing its formation and impacts, a multi-level perspective is essential. Using the STACKER 4D tracking algorithm and ERA5 reanalysis (2000–2023), this study provides a comprehensive climatology of shallow ETCs (2–3 pressure levels) across 12 levels (925–100 hPa) over the Southern Hemisphere (14° S–78° S). A total of 21,701 shallow systems were detected, representing 42% of all multi-level ETCs. Classification into three subfamilies, shallow low (SL, 925–600 hPa; 43%), shallow mid (SM, 500–250 hPa; 35%), and shallow upper (SU, 200–100 hPa; 22%), suggests a possible linkage with different physical mechanisms: surface baroclinic instability for SL, upper-level potential vorticity forcing for SM, and tropopause-level dynamics for SU. SM and SU systems, jointly accounting for 57% of shallow events, are unlikely to be detected by conventional single-level-based tracking methods. Three-level systems (S3) exhibit higher vorticity, longer lifetimes, and greater interaction with the UTLS region than two-level systems (S2), with implications for stratosphere–troposphere exchange. Maximum cyclone density is concentrated between 30–40° S and 50–60° S.

Keywords: extratropical cyclones; shallow family and subfamilies; Southern Hemisphere; tracking algorithm STACKER

Academic Editors: Fabrício Daniel Dos Santos Silva, Jório Bezerra Cabral Júnior and Gabriela Müller

Received: 20 April 2026
Revised: 11 May 2026
Accepted: 14 May 2026
Published: 16 May 2026

1. Introduction

Extratropical cyclones, usually referred to as ETCs, are dominant features of mid-latitude day-to-day weather variability in the mid-latitudes and their presence strongly impacts regional climates, as they are associated with extreme winds, large moisture gradients, temperature changes and precipitation [1–5]. In a climate that is expected to become warmer in the future, with more frequent severe events, a more accurate understanding of the cyclone behaviour and its changes is a significant and complex challenge, relevant for both immediate and long-term adaptation measures, especially considering

their potential economic and human impact [6,7]. This understanding must include not only their characteristics, location, intensity and frequency, but also their path, origin and evolution [8].

The first efforts to identify and understand extratropical cyclones were led by the Bergen School of Meteorology using the European telegraph network to track air pressure, temperature, and wind observations, describing the evolution of these systems on a continental scale for the first time. These observations gave rise to the well-known concept of fronts by Bjerknes in 1919 [9]. Since then, owing to their significant role in the poleward transport of heat and momentum, as well as the growing amount of information provided by reanalysis data over a long period of time, ETCs have been broadly researched across the globe, particularly over the Northern Hemisphere (NH) given the greater availability of data there. Current approaches are usually built around various automated tracking algorithms, analysing atmospheric data fields, in particular reanalysis data products, such as mean sea-level pressure (MSLP) and vorticity to identify cyclone centres as local minima in MSLP or maxima/minima in vorticity, depending on the hemisphere. Other key variables include geopotential heights, geostrophic vorticity, and relative vorticity, which can be used singly or in combination to detect and track atmospheric events globally [10–16].

The results of these different approaches on a global scale are not conclusive. Most of the results seem to agree that the total number of extratropical cyclones will decrease in the future [4,17–24], but there is no consensus on how the number of extreme cyclones will change, with some studies projecting an increase [17,20,25–27] and others a decrease [22]. As pointed out in [24], these differences may arise from the model used, the variable examined, the criteria and the selection of cyclones studied, as well as the geographic area under study.

At hemispheric scale, results tend to show that cyclones are projected to increase in intensity in the Southern Hemisphere (SH), but with a decrease in the Northern Hemisphere (NH) [18,21,24,26]. Yet, depending on the variable used, some authors observed increasing trends when mean sea-level pressure is examined, but others using vorticity show a very slight change or even a decreasing trend [24]. When geographical distribution is considered, comparing the hemispheres, cyclone density distribution is more zonally symmetric in the SH than in the NH due to the larger land masses and topographic features in the latter [28].

However, cyclone detection and tracking are highly complex and while strong, long-lived cyclones are typically better identified consistently, differences in the detection of weaker systems may arise depending on the tracking method, dataset, and resolution [29,30]. It is important to note that the vast majority of these results belong to analyses focusing on one or at most a few pressure levels, typically from gridded fields of sea-level pressure or 850 hPa geopotential height, but the vertical structure of tracked cyclones remains unclear even though it is known to play an important role in cyclone development and their impacts [15].

To date few analyses have examined the cyclonic systems at multiple pressure levels. In the SH, Lim and Simmonds [31] assessed the vertical structure of the cyclones in austral winter (JJA) from 1979 to 2000 by comparing tracks at six levels from mean sea-level pressure (MSLP) to 500 hPa. The study was based on cyclone tracks defined in terms of multi-level events by considering their variations in height, as well as sequences of multi-level overlaps defined for track points at different contiguous levels at a given timestep. Results were further separated into shallow systems up to 700 hPa and well-organised cyclones, at least up to 500 hPa. They found that cyclones are most commonly observed at the surface and at 500 hPa, with a minimum frequency value at 700 hPa with around 52% of the systems being considered "vertically well-organised", extending from the surface up to 500 hPa. On the other hand, Pepler and Dowdy [15] using the Lim and Simmonds [31]

methodology, studied the global distribution of cyclones at six vertical levels using mean sea-level pressure (MSLP) from ERA-Interim (ERA-I) reanalysis dataset. They found that about 50% of global cyclones show a coherent vertical structure extending to at least 500 hPa, while shallow cyclones were most common in the global midlatitudes. However, differences between the vertically well-organised and shallow systems' impacts still need to be further addressed [15].

More recently, based on the Hoskins and Hodges [13] single-level cyclone tracking algorithm, and with the aim of providing a more comprehensive picture of the cyclone events as time-evolving physical entities, we implemented a more complex 4D feature-tracking algorithm to track systems by analysing their entire 3D structure rather than just 2D features [32,33]. This approach combines tracks from different atmospheric levels into a single, integrated track, providing a multi-dimensional view of the cyclone's evolution over its lifecycle. This objective iterative method allows for a more comprehensive understanding of the cyclone's development by combining and stacking different levels of data, resulting in optimised 4D determination of relative vorticity anomalies. The analysis considered 12 pressure levels for systems track activity between 925 hPa and 100 hPa. As such, systems were classified into three main families, shallows, intermediates and deeps, on the basis of the maximum number of levels an event has at any stage during its lifetime. The research, derived from 17 years of ECMWF Reanalysis ERA-I dataset between 2001 and 2017, was focused on describing annual and seasonal characteristics of all the event occurrences between 14° S and 78 S. A complete overview of the results can be found in Lakkis et al. [33], where velocity, density, lifetime and vorticity among other characteristics were considered. Briefly, 58,231 multi-level events lasting at least 2 days with vertical structures spanning two levels or more were detected. Results from the whole sample showed that most of the events develop over the oceans rather than over land, and the 700 hPa pressure level plays an important role in the analysis, regardless of the family. During the whole period, the highest cyclone density was observed at mid-to-high latitudes, extending from the midlatitudes towards Antarctica, while high- and low-density values occurred over the South Pacific and over the Southern Central Indian Ocean, respectively. Areas with the highest density values were observed in regions associated with the polar jet instead of the subtropical jet. In terms of families, shallow events were found to be the most populated family followed by intermediate and deep cyclones, respectively. A clear distinction was also observed in the spatial distribution of densities among the three families. The shallow family cyclones were more frequently detected from the subtropics well into polar latitudes while intermediates extend from the extratropics into polar latitudes, and deeps were mostly sub-polar and polar. Regarding genesis and lysis of the events, shallow and deep systems tend to have a large percentage of genesis with their lowermost level at 925 and 700 hPa, while the intermediate ones have their genesis maxima near the surface and at 500 hPa. However, a refined analysis into each family considering subfamilies was not addressed at all, and this is a key aspect in order to advance in our understanding of cyclones and their impacts. Within each family, the vertical extent of a cyclone, i.e., the number of pressure levels over which cyclonic activity is detected, is not merely a geometric descriptor but a proxy for the degree of baroclinic coupling between atmospheric layers. According to potential vorticity (PV) theory, the development and intensification of extratropical cyclones depend critically on the interaction between upper-level PV anomalies and low-level temperature gradients [34]. Systems achieving coherent vorticity overlap across a greater number of pressure levels therefore imply a more advanced stage of baroclinic development and a stronger tropospheric column interaction, with direct consequences for their intensity, persistence, and capacity to transport heat and momentum poleward [3,35]. More vertically developed systems are generally longer-lived, more intense, and exert greater influence on

surface weather and upper-atmospheric dynamics, whereas systems with limited vertical extent tend to be more energetically constrained and shorter-lived [15,31].

Beyond vertical extent, the tropospheric layer in which a cyclone resides is closely linked to the physical processes governing its formation and impacts. Extratropical cyclones developing in the lower troposphere are predominantly driven by surface baroclinic instability and are closely associated with the passage of fronts, boundary-layer convergence, and strong surface pressure gradients; they are the primary contributors to extreme precipitation and surface wind events at midlatitudes [2,3,27]. In contrast, cyclones developing in the mid-troposphere are more likely to be associated with upper-level forcing mechanisms, such as potential vorticity anomalies propagating along the jet stream and troughs partially detached from the main westerly flow [34,36]. Finally, cyclonic systems residing in the upper troposphere and lower stratosphere represent a distinct class; they are more likely to correspond to cut-off lows or tropopause-level vorticity anomalies, with different formation mechanisms and the potential to influence stratospheric dynamics and stratosphere–troposphere exchange (STE) processes [36,37]. Recognising these distinct behaviours is essential for interpreting cyclone statistics in a climatologically meaningful way and motivates an approach that classifies systems not only by their horizontal and temporal characteristics, but also by their vertical location and extent within the tropospheric column.

Building on the multi-level climatology of Lakkis et al. [32], the present study focuses specifically on the shallow cyclone family in the SH, motivated by three key aspects: (i) What fraction of SH extratropical cyclones are structurally shallow, and how does their degree of vertical development, spanning different pressure levels, relate to their intensity, lifecycle, and capacity to interact with the upper troposphere and lower stratosphere (UTLS)? (ii) Do shallow cyclones occurring in different tropospheric layers represent distinct classes of systems with different formation environments, spatial distributions, and potential weather impacts? (iii) What does a comprehensive 24-year multi-level climatology of shallow events, spanning 12 pressure levels from 925 to 100 hPa, reveal about the population of extratropical cyclones that remain undetected by conventional single-level-based tracking approaches?

To address these questions, annual statistics of cyclone frequency, translational velocity, relative vorticity, lifetime, track density, and genesis and lysis levels are examined across the 14° S–78° S latitudinal band using the ERA5 reanalysis dataset for 2000–2023 and the STACKER multi-level tracking algorithm [32,33]. The manuscript is organised as follows: Section 2 describes the data and methodology; Section 3 presents the results for the shallow family and its subfamilies; and Section 4 provides an integrated discussion and concluding remarks.

2. Data and Methodology

The data used in this study are from the ERA5 reanalysis obtained from the Copernicus Climate Change Service which is the newest atmospheric reanalysis produced by the European Centre for Medium Range Weather Forecasts [38], and it is based on the Integrated Forecasting System (IFS; cycle 41r2). The dataset has a horizontal resolution of 31 km, and vertically it has 137 levels from the surface up to approximately 80 km and provides hourly analysis and forecast fields, covering from 1950 onwards. In the present study fields of relative vorticity (RV) at 6 hourly intervals were used from 2000 to 2023.

The present study closely follows the methodology established in the previous SH cyclone tracking studies by Lakkis et al. [32,33], and it draws from concepts introduced in Lim and Simmonds [31] and Hoskins and Hodges [13]. The range of pressure fields where the systems are explored ranges between 925 hPa and 100 hPa and the area spans

the latitude band between 14° S and 78° S. Although the entire detection and tracking process can be read in unabridged form in the previous manuscripts, it is worth mentioning some details here. The tracking is performed using the STACKER algorithm involving single-level cyclone tracks obtained with the Track algorithm [39,40] for 100, 125, 150, 200, 250, 300, 400, 500, 600, 700, 850 and 925 hPa pressure levels. The methodology considers that potential cyclone centres at a given level are initially identified in the T42 filtered data as minima for SH by comparing the relative vorticity values of each grid point to its neighbouring grid points and then refined to find their off-grid locations using B-splines and steepest descent minimization [39]. The cyclones are allowed to have any lifespan at a given level, but multi-level events are only retained when they persist for at least 2 days. The relative vorticity threshold used is -1.0×10^{-5} s^{-1} at all levels. Using the objective function criterion, the STACKER algorithm associates all tracks obtained from a given single-level feature-tracking algorithm that represents the same synoptic event at different vertical levels. The process is performed iteratively over adjacent pressure levels until the stacking of tracks is complete. The analysis is based on cyclone tracks defined in terms of multiple-level events by considering their variations in height, as well as sequences of multi-level overlaps defined for track points at different contiguous levels at a given timestep (whose coordinates at an immediate upper level fall within a 4° latitude radius [≈444 km] of the track point being considered at the lower level). The algorithm works both bottom-to-top and top-to-bottom, capturing such features as upper-level troughs or cut-off lows. It is worth mentioning that both bottom-to-top and top-to-bottom procedures resulted in highly consistent detections between each other.

To improve the analysis of the vertical extent of the systems, detected cyclones are classified into families and broken down into subfamilies or subtypes. It is relevant to emphasise here that, to reinforce the idea that cyclones are physical entities rather than sample slices at specific pressure levels, the classification into families is based on the most frequent number of pressure levels that an event has at any stage of its lifetime. That is, the family classification is based on the most frequent value of the vertical extent observed across all timesteps of the system's lifecycle: the number of levels that the system most frequently exhibits, rather than the maximum it ever reaches. This ensures that the classification reflects the system's typical three-dimensional configuration rather than an occasional or transient state. Family classification was defined as shallow (2–3 levels), intermediate (4–5 levels) and deep (at least 6 levels) and further subdivided into subfamilies, or subtypes, depending on the height ranges of the pressure levels where the entities are detected. To better illustrate the concept, the reader may refer to the schematic diagram of families and subfamilies provided by [41] in their Figure 2, where a cyclone is represented as a cylinder with the base and top denoting its lower and upper pressure levels, respectively. However, there are several key differences between the two approaches that must be noted: the classification into families and subfamilies and the pressure levels assigned to each of them are different; Yao et al. [41] set up the "radius" of the cylinder or searching range in 555 km whereas in our case it is fixed at 444 km, and the events considered in this analysis have no minimum trajectory length restriction. The present analysis is restricted solely to the shallow family and its subfamily is defined as shallow low, middle and upper, covering pressure levels of 925–600, 500–250 and 200–100 hPa, respectively.

The cyclone properties analysed are track density, translational velocity, vorticity, lifetimes, genesis and lysis areas. All variables are plotted at 2° × 2°-pixel resolution for the full study area. In the case of track densities, these are corrected for cell central latitude, so that the density refers to equal-area pixels. The number of events occurring on each pixel are further expressed as mean annual values. Lifetimes are obtained by considering the times and dates of the first and last positions of each cyclone event. These values are

then assigned to the cells over which the cyclone event moved. All the lifetimes in each cell were then averaged. The translational velocity and the vorticity are calculated at each timestep and pressure level in a given event and averaged in height and assigned to the corresponding cell at each timestep. All values for events in each cell were then averaged. Genesis and lysis density distributions are also considered. As in previous analyses, the first (last) position of the event is considered for genesis (lysis) plots; but, in order to develop a more comprehensive picture of the vertical structure of the entity in the present approach, we have also determined the lower and upper levels of genesis and lysis.

Finally, the trend of cyclone frequency is obtained using the linear regression method calculated from least-squares. The Mann–Kendall (MK) non-parametric test of statistical significance [42] is used as an indicator of the statistical significance of the trend at the confidence level of 95%.

3. Results

3.1. An Overview of the Shallow Family Distribution

Throughout the study period, a total of 51,430 multi-level events were detected, with 21,701 of them belonging to the shallow family. That is approximately 904 events per year and around the 42% of the total events, a percentage that, although lower than that recorded in Lakkis et al. [33] using the ERA-I dataset for the period 2001–2017, also shows that shallows are still the family with the highest number of events. As was mentioned above, many authors have noticed that results may vary depending on the database used, even using the same methodology for detecting and tracking cyclonic systems; these discrepancies not only impact cyclone detection but also several other topics. For instance, during 2017, Hoffmann et al. [43] observed differences between transport simulations using ERA5 and ERA-I data as large as 3K in temperature, 30% in specific humidity, 1.8% in potential temperature, and 50% in potential vorticity after 1 day. McErlich et al. [44] compared the output from the ERA5 reanalysis with WindSat data to identify the similarities and differences in the cyclone characteristics between these two products. They found that the ERA5 reanalysis underestimated precipitation in the warm sector of SH extratropical cyclones while overestimating it in the cold sector and cloud liquid water in the cold sector, resulting in some biases in the frequency and lifetime of the detected systems. On the other hand, Marrafon et al. [45] examining extratropical cyclones in the SH, showed differences in magnitude and significance of the detected trend of the annual frequency between ERA-I and ERA5. Due to the high spatial and temporal resolution of the ERA5 dataset, it is also plausible to hypothesise that some of the events previously detected with ERA-I as shallows are now observed as having a larger vertical extent and therefore fall into another family.

The frequency distribution per year is shown in Figure 1a. The maximum number of events is detected in 2011 (978), while the minimum is observed during 2012 (842). Even though the number of events appears to decrease very slightly over time, no significant trend is observed through the MK test. The figure could suggest the existence of decadal to interdecadal variability. If the vertical extent is considered, from Figure 1b, it is clear that shallow systems developing in two levels are the most populous group, with almost 13,000 cyclones detected.

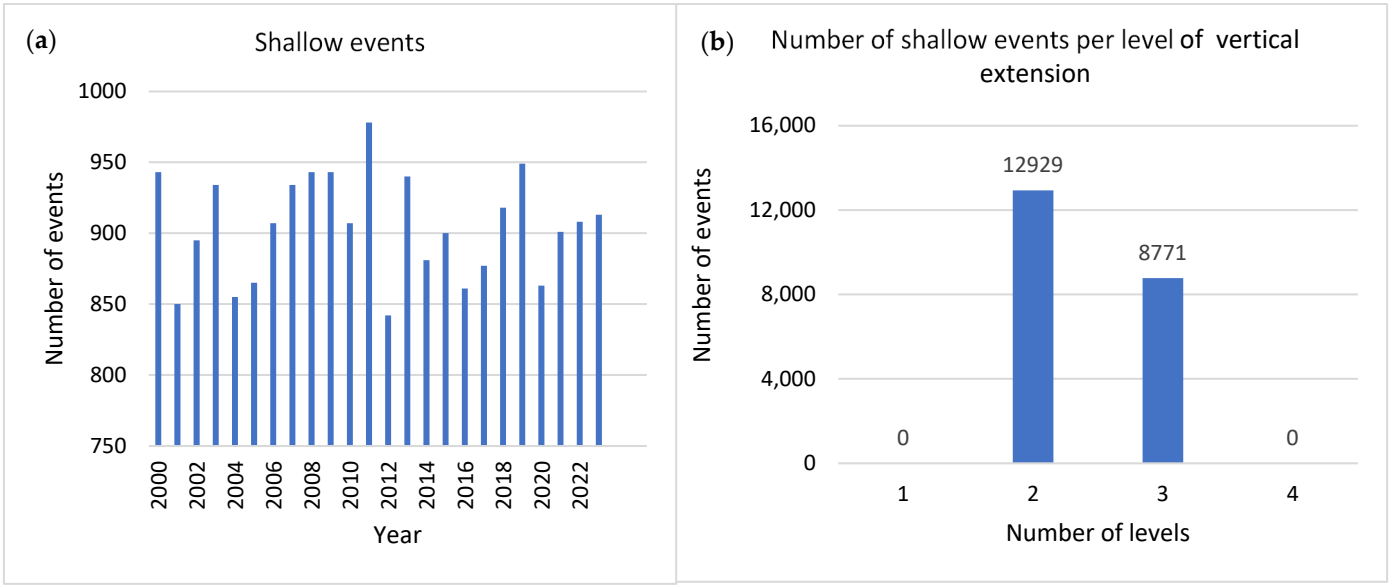

Figure 1. (**a**) Number of shallow events per year over the period analysed and (**b**) number of events with 2 and 3 levels of vertical extent.

A preliminary inspection of the frequency distribution given in terms of the lowermost pressure level per event, constructed by assigning an event, determined by STACKER to the lowermost level present during its lifecycle, shows a clear maximum value at 925 hPa (Figure 2a). Above 700 hPa and up to 300 hPa, the distribution is roughly constant in terms of events at each pressure level, although there is a relative maximum at 500 hPa with 1940 events detected. Fewer systems are observed to have their lowermost level in the upper troposphere/lower stratosphere (UT/LS), with the absolute minimum value at 125 hPa (307 cyclones). Thus, close to 50% of the observed systems occur near the surface, while around 40% of cyclones have their lowermost level in the mid-troposphere up to 300 hPa. Comparison with other results appears challenging as there are no studies involving this many pressure levels and focusing on just shallow events. However, in general terms, the distributions are consistent with those obtained in the previous analysis using the ERA-I dataset. Figure 2b shows the distribution for the uppermost levels. Here, the difference between maxima and minima narrows and the distribution is slightly more homogeneous, but with the absolute maximum values at 125 hPa with 5400 cyclones. High values are also observed at 250 and 200 hPa, as well as close to the surface at 850 hPa and 700 hPa. In light of the results, and considering that the corresponding pressure ranges of the tropopause are about 150 to 320 hPa at the SH [46,47], it is clear that, although ETCs were thought to be predominantly a tropospheric phenomenon, many of them can "punch up" into the lower stratosphere, influencing the upper atmosphere's structure and dynamics and even involving some stratosphere–troposphere exchange. Hirschberg and Fritsch, as early as 1991 [48], postulated that the tropopause undulations can influence the extratropical cyclone development by creating temperature and potential vorticity anomalies and acting synergistically with the developing cyclone, intensifying the vertical circulation and contributing to the storm's growth. These events developing upward into the stratosphere may fall into the upward-stratospheric explosively developing cyclone category (US-EC) defined by Qian et al. [49]. According to their statement, these US-EC systems, originating in the lower troposphere, can pass through the tropopause and exhibit significant vertical development extending into the stratosphere. From a broader perspective, Canziani and Legnani [50] presented observational studies analysing the local circulation conditions that allowed for tropospheric synoptic-scale systems to extend

beyond the tropopause into the lower stratosphere, up to 100 hPa. Nathan and Hodyss [51] provided a theoretical framework based on an extended Charney–Drazin condition to explain such observational results. We will touch on this topic again later in the analysis.

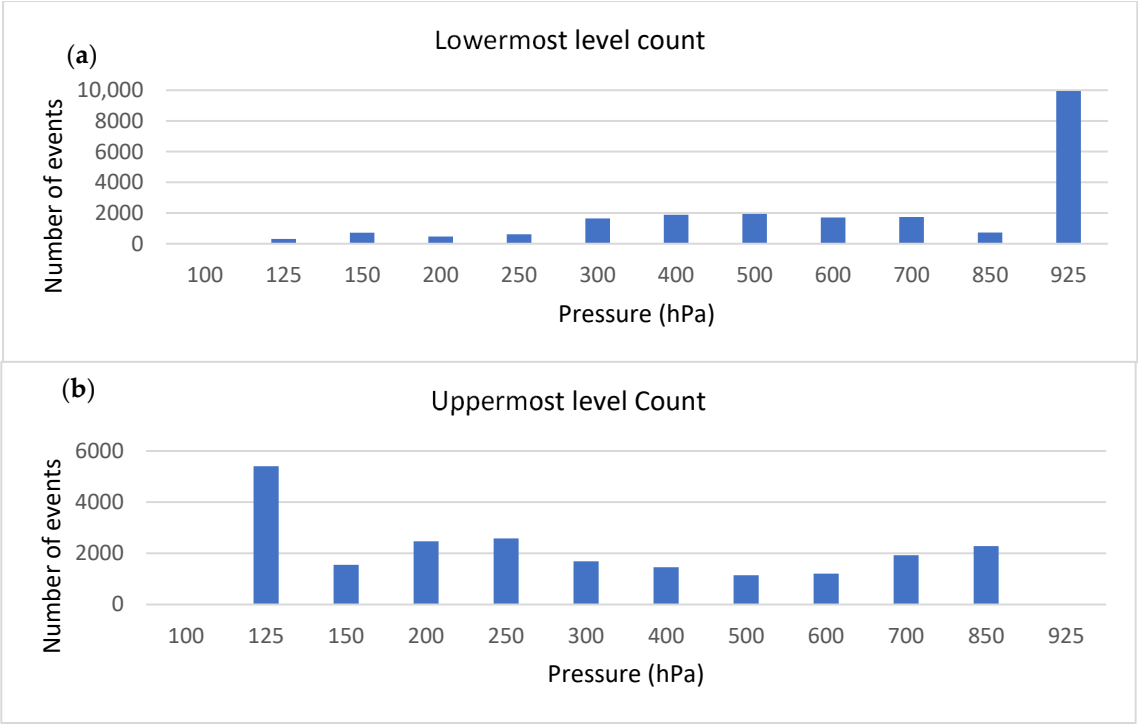

Figure 2. Histogram of the (**a**) lowermost and (**b**) uppermost level distribution for shallow events. The histograms are constructed by assigning an event to the lowermost (uppermost) level present during its lifecycle.

Figure 3 shows the mean values of the lifetime, vorticity, velocity and distance travelled for the shallow family over the 24 years under study. According to the results, the systems live for on average 4.27 days (Figure 3a), with mean velocity values of around 12.5 m/s, and a mean distance travelled of around 3229 km (Figure 3b,c). Mean vorticity values (Figure 3d) have been observed to be close to 4.6×10^{-5} 1/s. The values appear to be consistent with [31] and [33], but somewhat higher. As mentioned above, differences may arise due to the seasonal time in which the analysis is performed, the number of pressure levels considered, the use of different variables to track systems instead of vorticity, and different datasets and sampled periods.

The frequency histograms corresponding to genesis and lysis levels of the shallow cyclone activity throughout the year and for the entire period of study are shown in Figure 4. In line with the idea of addressing cyclone behaviour as physical entities with a defined vertical 'structure' given by the maximum vertical extent, frequency histograms have been developed for the lower- and uppermost levels of genesis (Figure 4a,b) and lysis (Figure 4c,d). That is, considering the lower and upper level of their first and the last appearance defined as the lower and upper first (last) point identified by the algorithm.

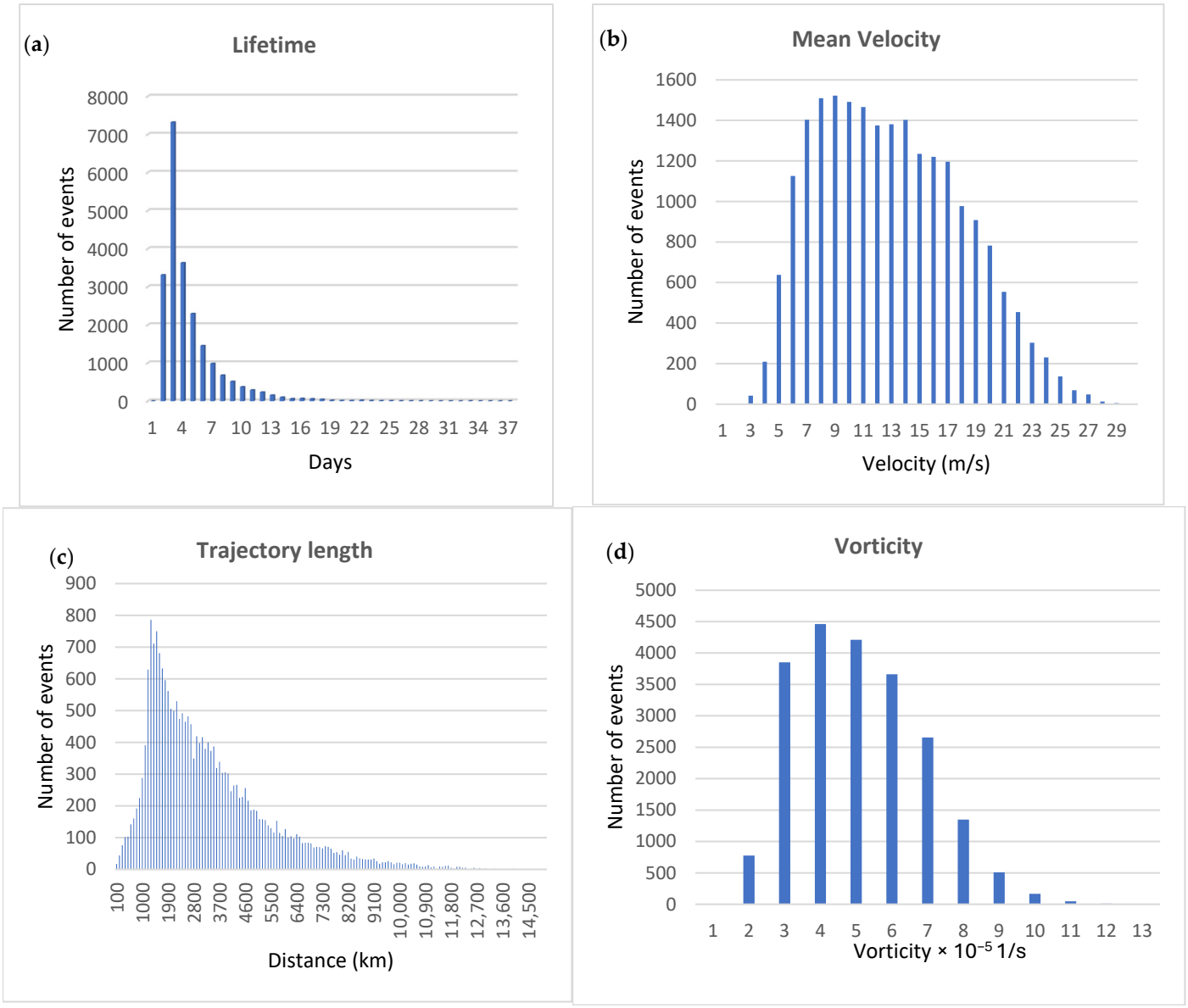

Figure 3. Mean values of lifetime in days (**a**), mean velocity in m/s (**b**), trajectory length in km (**c**) and vorticity in 1/s (**d**) for the shallow family events during 2000–2023.

According to the results, almost 31% of the systems have their lowermost genesis level near the surface at 925 hPa; while less than 17% can be observed in the stratosphere. At mid-range pressure levels, the number of events shows an increasing distribution between 850 and 300 hPa, above which the number of systems decrease until reaching their minimum at 125 hPa (Figure 4a). Uppermost genesis levels (Figure 4b) show maximum values also near the surface but a high number of the events are concentrated in the UTLS, being the minimum at 150 hPa. On the other hand, frequency distribution of the lysis levels (Figure 4c,d) is quite similar for both the lower- and uppermost level, except for the number of events detected at 125 hPa. While at the lowermost lysis level, the number of events is closely to the absolute minimum value observed at 850 hPa, for the uppermost level, there are almost the same number of events as at the absolute maximum value at 925 hPa.

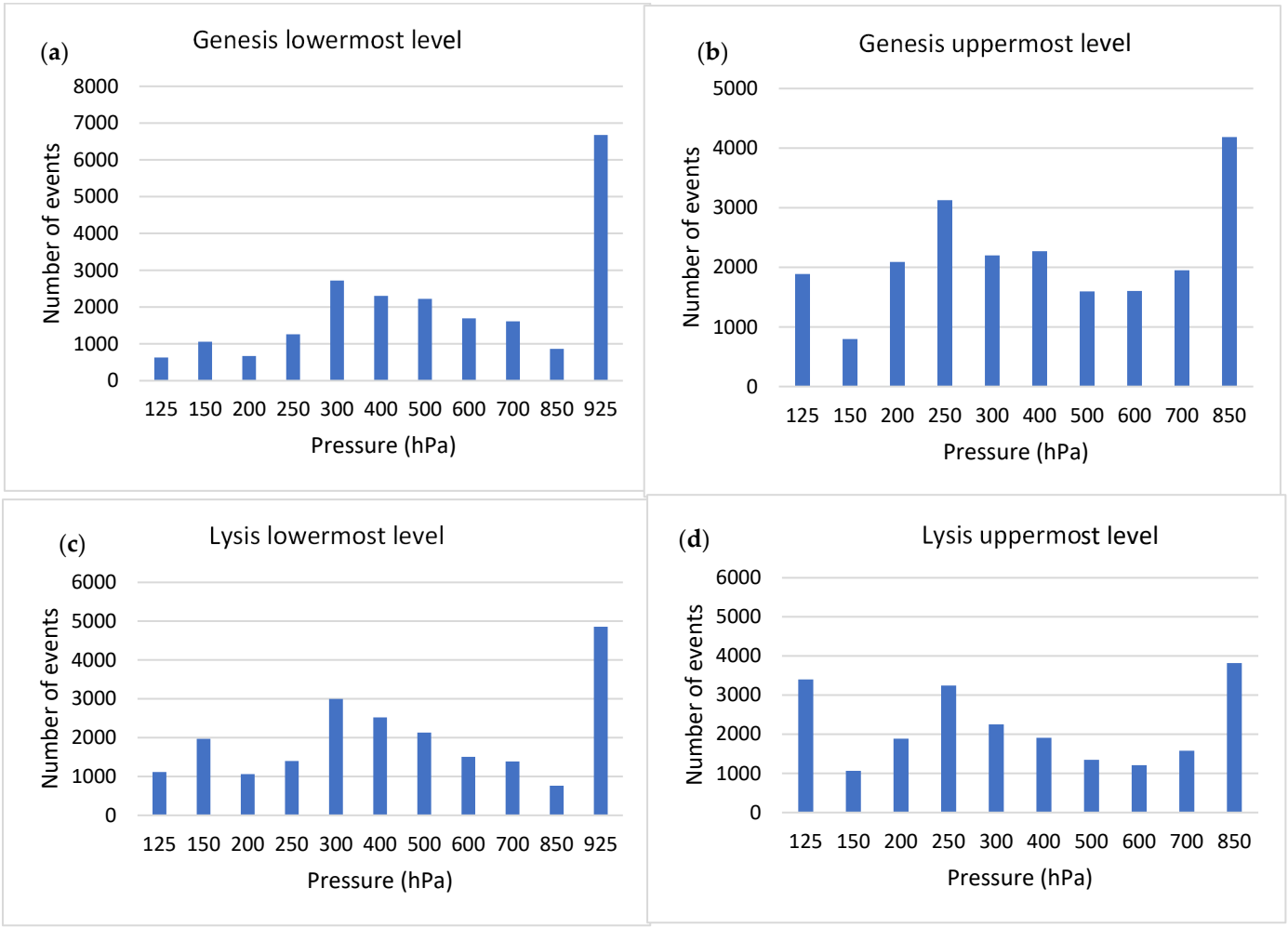

Figure 4. Lowermost and uppermost genesis (**a**,**b**) and lysis (**c**,**d**) for the shallow family for the 2000–2023 period.

A simple additional analysis using both the lower and upper levels of both genesis and lysis can reveal a slightly clearer picture of the behaviour of these shallow events, particularly related to their vertical extent and their dynamic. Figure 5 shows the distribution by pressure levels of the difference between the lowermost and uppermost level, both for genesis (a) and lysis (b).

As expected, since we are dealing here with shallow events that can develop at most at three levels, the histograms show for each lowermost level (the base of the cyclones structure and where the events birth (y axis)), a two-colour combination corresponding to the most frequently uppermost levels detected. For example, systems with their birth at 925 hPa (Figure 5a), display their decay (uppermost levels) at 850 hPa and 700 hPa. A similar procedure made with lysis levels show that most of the events with their lowermost level at 925 hPa (Figure 5b), display their uppermost level at 850 hPa and 700 hPa.

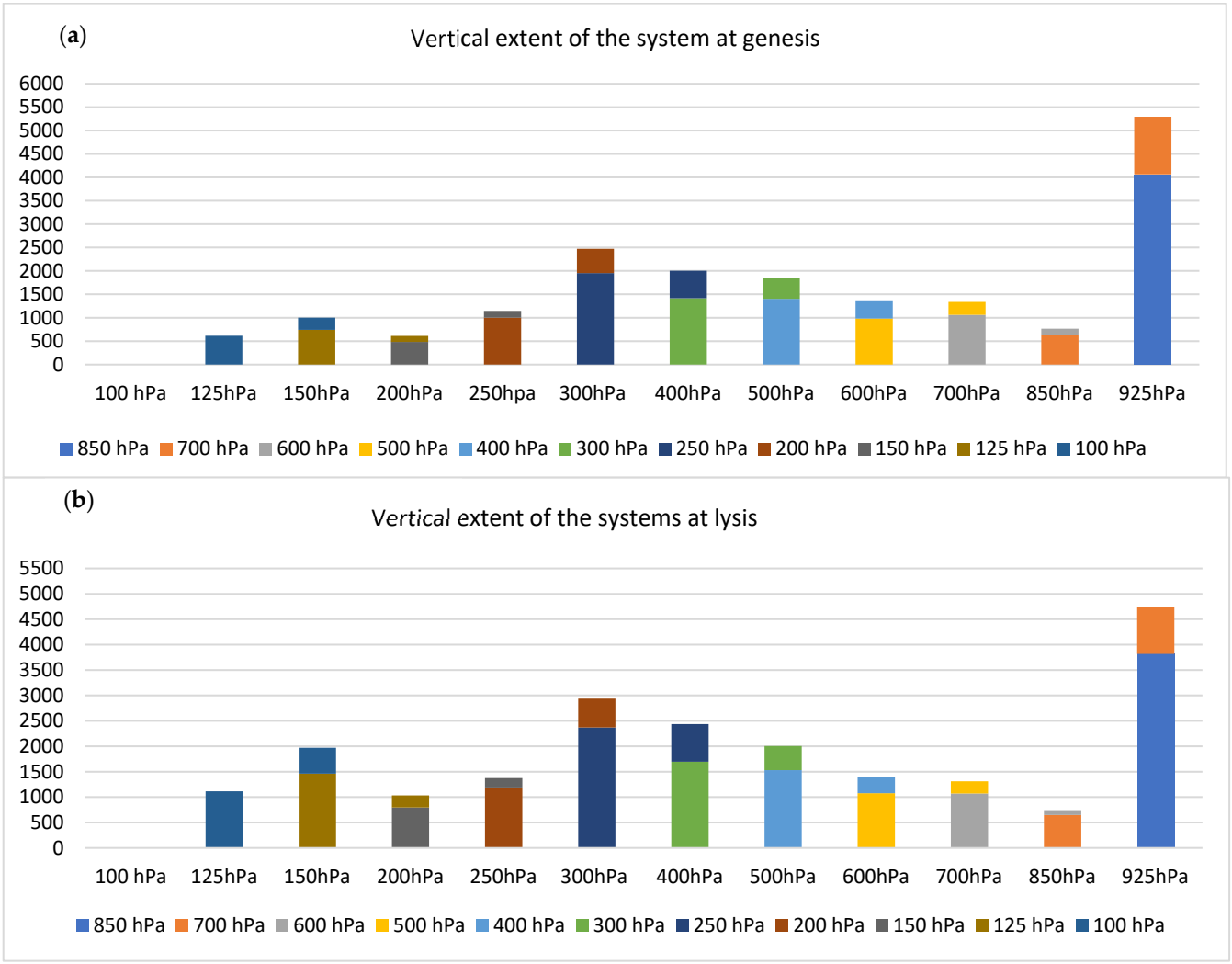

Figure 5. Vertical extent of the systems in the genesis (**a**) and lysis (**b**) stages. Plots were constructed by subtracting the upper level to the lower level-the last one considered as the base of the event of the genesis (lysis).

At first glance, the histograms show results that reinforce those obtained in Figure 4: most of the shallow systems usually have their genesis and lysis close to the surface and in the middle troposphere, with decreasing number in higher altitudes, meaning that the tropopause plays a key role in the development of systems, acting as a barrier that slows down their move towards the stratosphere. However, it should be noted that the number of systems whose genesis and lysis can be observed at lower stratospheric levels is not negligible. As mentioned above, the cyclones, particularly shallow events, weaken and tend to dissipate on the ground or at the tropopause as they lose energy and upper-level divergence decreases; nonetheless, there is well-documented evidence of events that cross the tropopause barrier and reach the stratosphere, modifying the tropopause structure and dynamics as well as stratosphere–troposphere exchange (STE) processes in the upper troposphere and lower stratosphere (UTLS) region [52–54]. However, it should be noted that, since the STACKER algorithm detects cyclonic systems based on relative vorticity anomalies without distinguishing their formation mechanisms, some of the detected shallow systems, particularly within the SU subfamily, may correspond to isolated low-pressure systems or cut-off lows (COLs). These low-pressure systems are usually closed circulations in the middle and upper troposphere developed from a deep trough in the westerlies [55]. They are usually smaller than extratropical cyclones during its

mature phase and have a lifecycle of around 2 to 3 days, although their duration can be as long as 5 days. The main difference between COLs and ETCs is the developing mechanisms. While COLs become completely detached from the jet stream, the cyclone events usually remain connected to the basic westerly flow. Given that the purpose of the results shown in Figure 5 is to present basic statistics on shallow events, delving deeper into the mechanisms of formation and therefore distinguishing both classes of systems is beyond the scope of this study as it would require additional dynamical information not available in the present framework, such as an explicit analysis of jet stream detachment or upper-level potential vorticity fields.

Figure 6 shows the relation between velocity, lifetime and distance travelled for the shallow events. As may be expected, and in accordance with previous results with ERA5 [33], those systems with higher velocity tend to travel larger distances (Figure 6a), while (Figure 6b) ETCs with shorter lifetime tend to be faster.

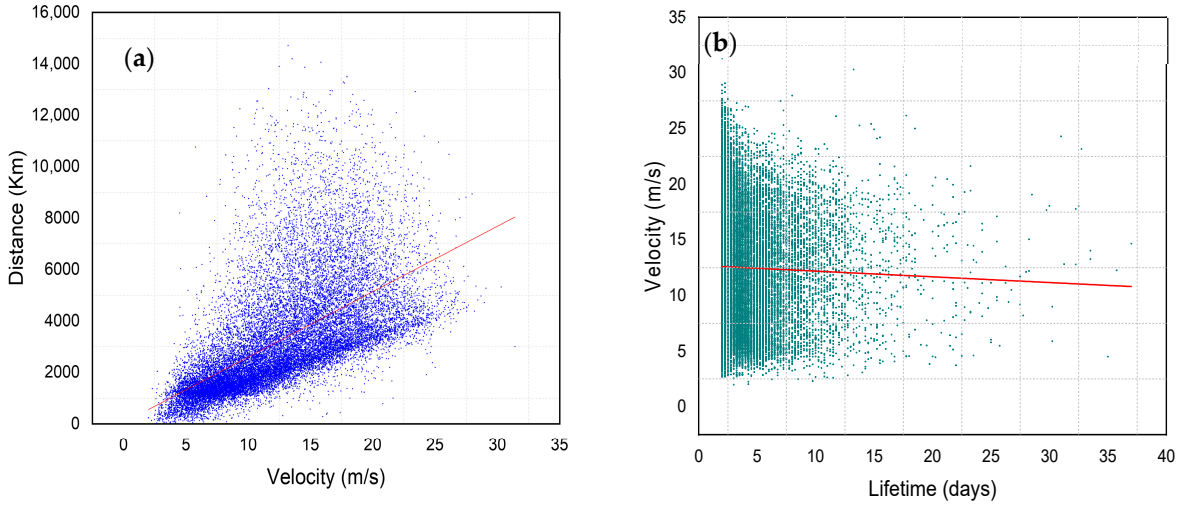

Figure 6. Relationship between (**a**) distance (km) and velocity (m/s) and (**b**) velocity (m/s) and lifetime (days) for shallow events. The red line shows the linear fit.

3.2. Picturing Shallow Events by Number of Levels

Before proceeding further and focusing on the characteristics of the subfamilies, it is interesting to note the differences and similarities between shallow events developed at two (hereafter S2) or three (hereafter S3) levels of vertical extent. As mentioned in Figure 1, the most numerous group of shallow events corresponds to systems with two vertical levels. Both of them display distributions per events and years with no significance trends detected.

Figure 7 shows the distribution of velocity, trajectory length and vorticity for events S2 (left panel) and S3 (right panel). The lifetime is not shown in the figure because the difference is barely noticeable in the distribution, but the results account 4.13 days for the S2 systems and 4.46 days for the S3. The results also indicate that S2 are on average almost 1 m/s slower than the S3, with a left-skewed distribution in which most systems are clustered on the right side with values ranging between 7 and 17 m/s (Figure 7a). The probability decreases slowly at first but drops sharply from 19 m/s onwards. In contrast, S3 events present a near-Gaussian behaviour, with values around the mean average of the order of 13 m/s (Figure 7b). A similar behaviour can be found when trajectory length is observed. Both, S2 and S3 systems show a left-skewed distribution, although higher values are more frequently observed in S3 distribution. On average more S3 systems travel larger distances. Average and maximum values are found to be around 3090 and 1300 km for S2 and 3440 and 1700 km for the S3. As far as vorticity is concerned, the difference is

more remarkable. Most of the S3 vorticity values, displaying a quasi-normal distribution behaviour, are higher than S2 cyclones with average values around 4.4 and 4.8 × 10^{-5} 1/s, respectively. Following the same criteria as in Figure 6, Figure 8 shows the difference between the lowest and uppermost level for the events, but for systems per number of levels (S2 and S3). As expected, the behaviour of the genesis and lysis of two- and three-level systems closely follows the same pattern as that of the entire family (Figure 5), with most of the cyclones with their genesis near the surface and decreasing above 300 hPa near the tropopause. However, this decrease appears to be slightly more noticeable for S2s than for S3s, given that two-level events account for 60% of shallow systems (Figure 1b). It is particularly interesting that S3s have a higher percentage of their lysis stage near and beyond the tropopause than S2 systems.

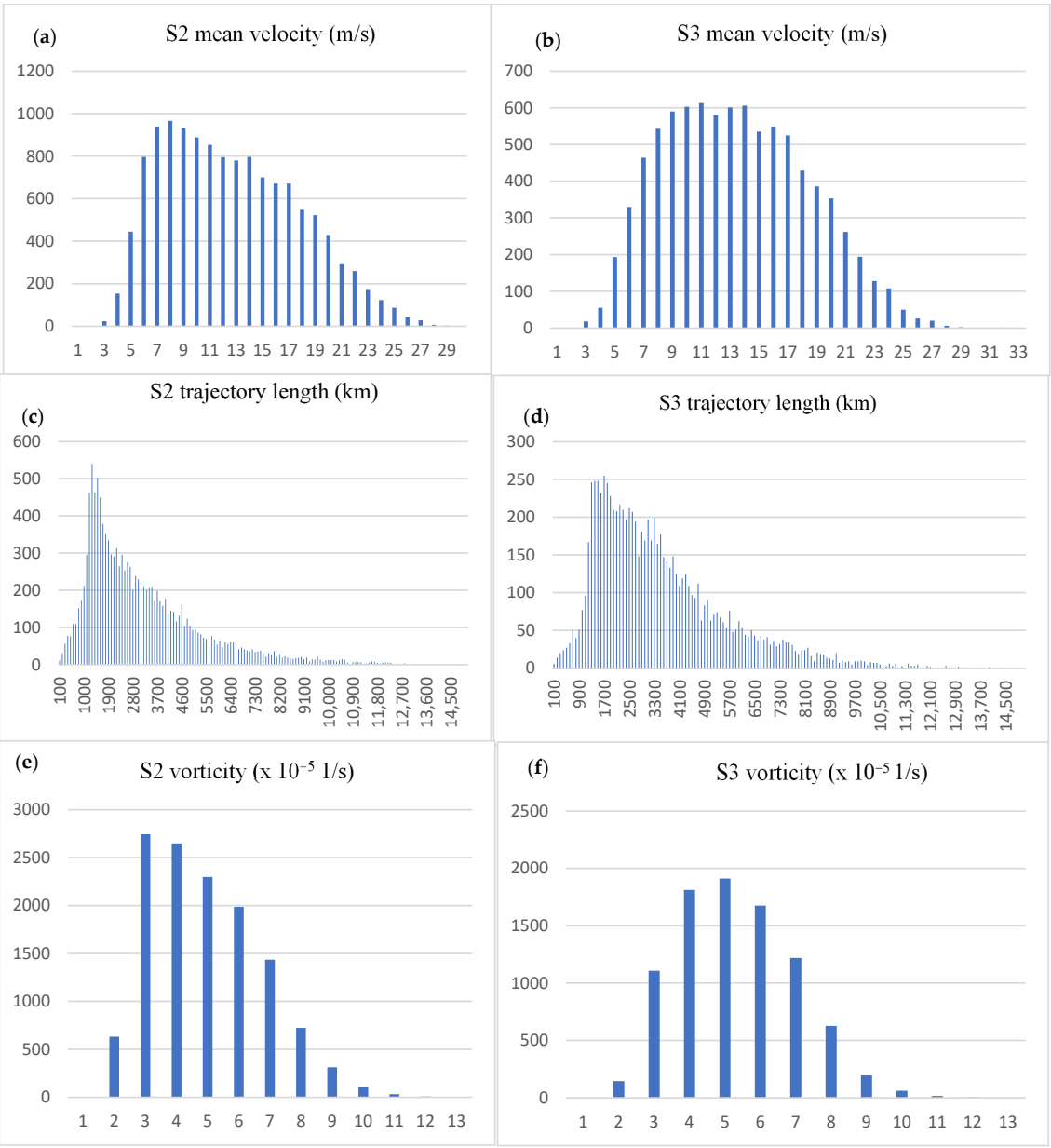

Figure 7. Velocity, trajectory length and vorticity for shallow events with 2 levels (left panel (**a**,**c**,**e**)) and 3 levels (right panel, (**b**,**d**,**f**)) of vertical extent. Note the differences in the scales for better viewing.

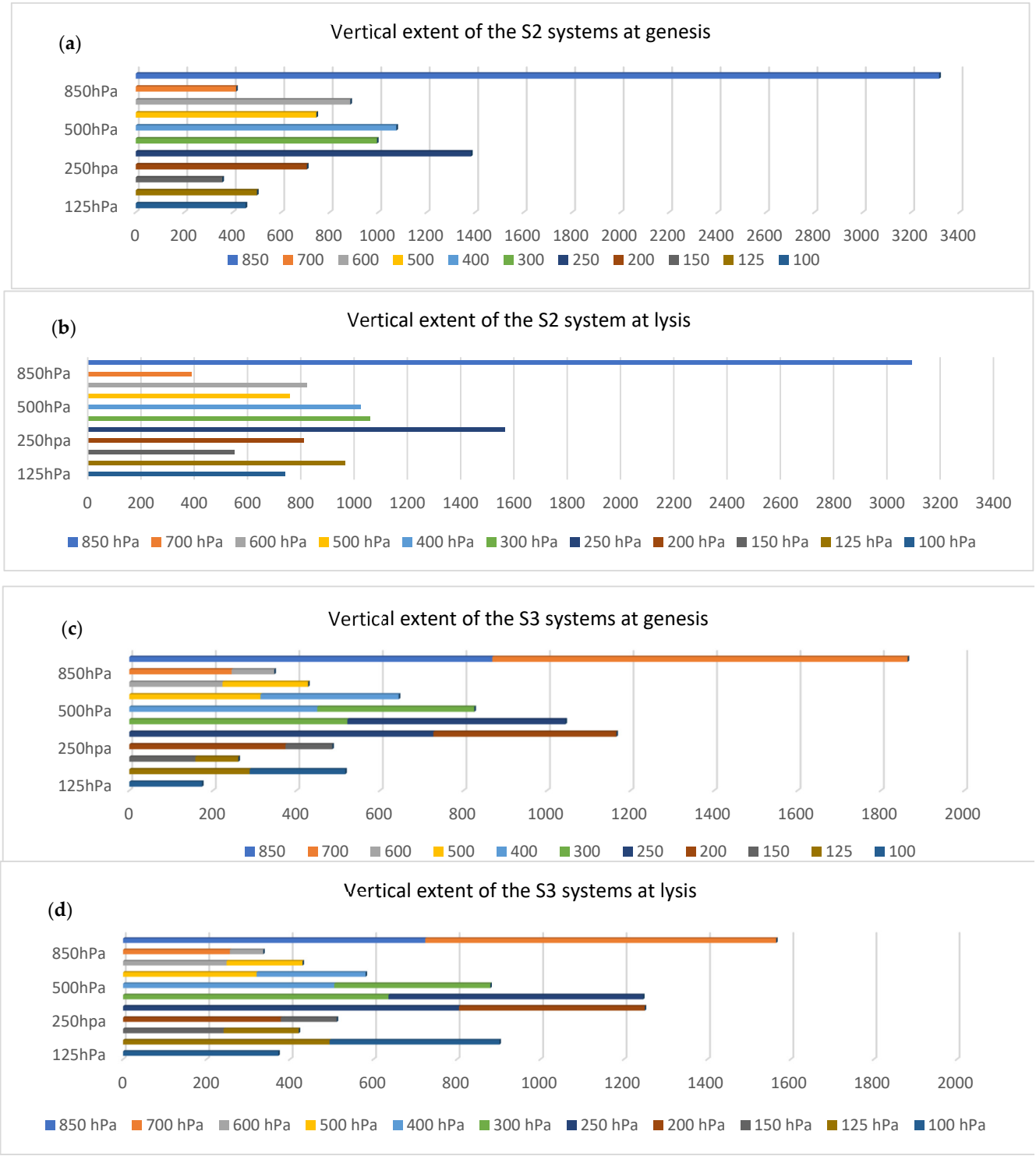

Figure 8. Histograms of vertical extent at genesis and lysis of the S2 (**a**,**b**) and S3 (**c**,**d**) systems constructed as the difference between the lower- and uppermost levels.

These differences between S2 and S3 systems suggest that the distinction is not merely statistical but may reflect underlying dynamical differences. Within the framework of baroclinic development theory [34], the additional level of vertical coherence in S3 systems is consistent with a stronger interaction between the upper-level potential vorticity anomaly and the low-level baroclinic zone and, consequently, greater vorticity amplification and longer system persistence (Figure 7d,f). The different velocity distribution shapes (left-skewed for S2 and quasi-Gaussian for S3), further suggest that these two subtypes do

not simply represent different stages of the same developmental process, but may arise from different large-scale forcing environments or initial conditions. More critically, the high proportion of S3 lysis events at or above the tropopause implies that three-level shallow cyclones are the subgroup most capable of interacting with the UTLS region. This has potential consequences for stratosphere–troposphere exchange (STE); when cyclonic circulation reaches tropopause levels, it can induce tropopause folding and downward transport of ozone-rich stratospheric air into the troposphere [37,56], a process relevant for both atmospheric chemistry and upper-tropospheric dynamics. In contrast, S2 systems, being more energetically limited and predominantly confined to the lower and middle troposphere, contribute less significantly to UTLS dynamics but account for the majority of shallow cyclone activity (60%) and therefore constitute the dominant mode of shallow cyclone activity across the SH midlatitudes.

3.3. Subfamilies Results

The shallow family was further subdivided into three subfamilies according to the lowermost pressure level of the system during its lifetime: shallow low (SL; 925–600 hPa), shallow mid (SM; 500–250 hPa), and shallow upper (SU; 200–100 hPa). This subdivision is relevant since the atmospheric layer in which a cyclone resides is closely linked to the dominant dynamical processes driving its formation, structure, and dissipation. SL systems develop within the planetary boundary layer and lower troposphere, where baroclinic instability is primarily driven by surface temperature gradients, frontal dynamics, and boundary-layer convergence; they are the class most directly linked to surface weather impacts including extreme precipitation and surface winds [2,3]. SM systems, located in the free troposphere between 500 and 250 hPa, are more closely associated with upper-level forcing mechanisms, potential vorticity anomalies propagating along the jet stream, and cold closed lows that have become partially detached from surface baroclinicity [34,36]. SU systems, residing in the upper troposphere and lower stratosphere between 200 and 100 hPa, represent a dynamically distinct class more closely related to cut-off lows and tropopause-level anomalies, with formation mechanisms that differ fundamentally from classical surface baroclinic development and with potential implications for stratosphere–troposphere exchange [36,37]. Crucially, both SM and SU systems are not captured by conventional single-level or MSLP-based tracking methods, which means they are absent from the majority of existing SH cyclone climatologies, a significant gap that the present multi-level approach is designed to address. Figures 9 and 10 and Table 1 summarise the main characteristic values on average for each subfamily.

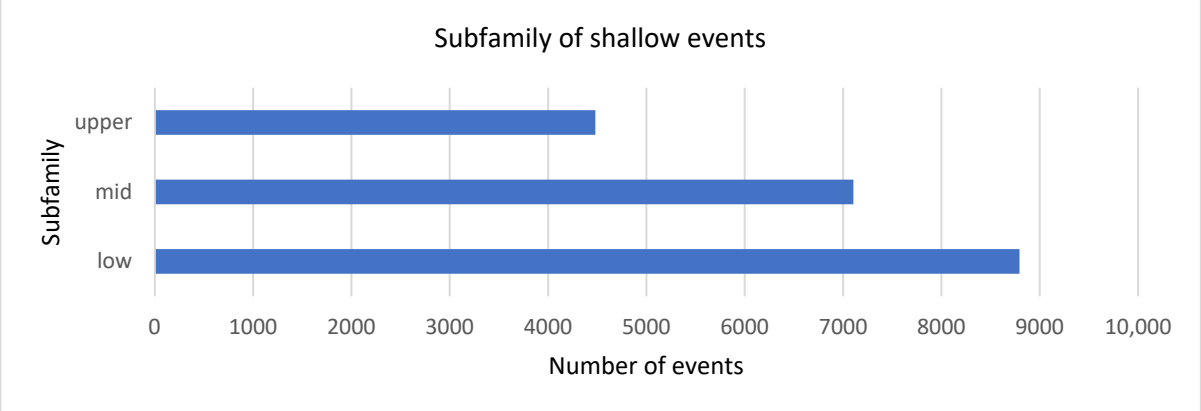

Figure 9. Number of shallow events per each subfamily.

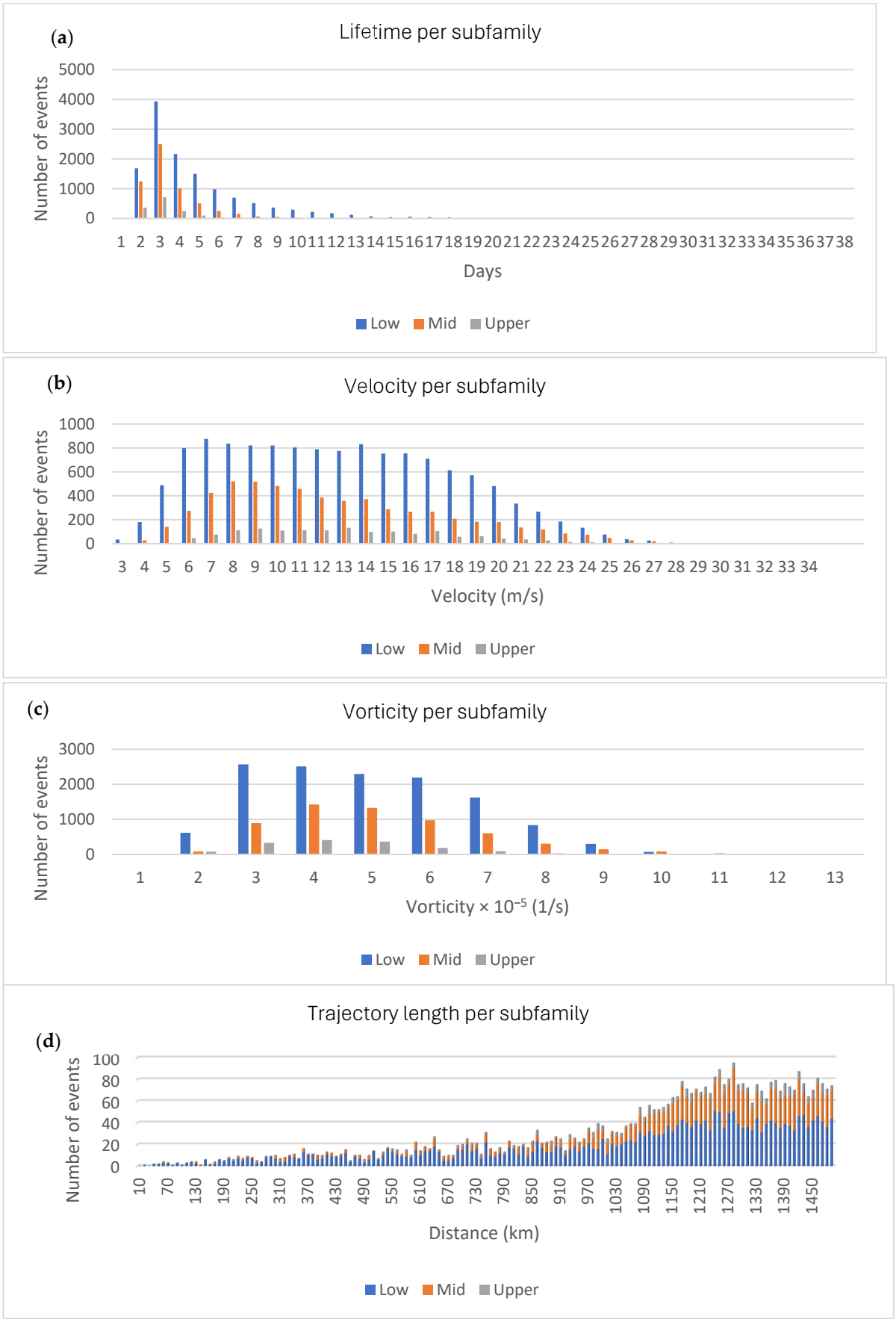

Figure 10. Frequency distribution of velocity (**a**), lifetime (**b**), vorticity (**c**) and trajectory length (**d**) for each subfamily.

Table 1. Average values of the main characteristics for each subfamily of shallow systems. Maximum values are highlighted in yellow.

Subfamily	Velocity (m/s)	Lifetime (Days)	Vorticity $\times 10^{-5}$ 1/s	Distance Travelled (km)
SL	12.4	4.64	4.6	3406
SM	12.2	3.25	4.6	2590
SU	12.6	2.87	4.0	2395

As with all the family of shallow cyclones (Figure 1a), the histogram of the distribution of event counts by year and subfamily does not yield a significant trend over time, and the number of events remains relatively constant. Based on the results from Figure 9, SL systems are the most frequently detected, accounting for 43% of the total sample, while SM and SU events account for 35% and 22%, respectively.

The distribution of the main characteristics for each subfamily and the mean values are shown in Figure 10 and Table 1. According to the histograms, the lifetime (Figure 10a) exhibits a similar behaviour to that of the entire shallow family, with a left-skewed distribution and maximum values of around 3 days for all the subfamilies. On average, SL events are the longest-lived system with a lifespan of almost 4.7 days. Including all the subfamilies, lifespan range is similar to that described by Simmonds and Keay (2000) [28] in their climatology of SH extratropical cyclones, although they also considered systems with a minimum duration of one day. Regarding the behaviour of the velocity (Figure 10b) the overall distribution is somehow right-skewed and the number of events is the highest at lower velocities and gradually decreases as velocity increases. Most events occur between 3 and 20 m/s, with very few beyond 25 m/s and virtually no events occur beyond 27 m/s. With regard to subfamilies, the SL subfamily dominates the distribution, reaching its maximum around 7–8 m/s with approximately 800–900 events, and then decreasing steadily beyond 15 m/s. The SM subfamily peaks slightly later, around 8–9 m/s, with about 500 systems, and decreases more rapidly afterwards. Finally, SU systems remain consistently low, with fewer than 150 cyclones at all speeds. According to Table 1, although SU systems are the fastest, the differences in the average values for each subfamily are unremarkable, and the systems travel at an average velocity of approximately 12 m/s. The results are consistent, although slightly higher than those obtained by [15], who, using mean sea-level pressure (MSLP) data from the ERA-Interim reanalysis as a tracking variable, studied systems between 925 hPa and 500 hPa. They found an average speed of around 10 m/s. The mean values are also similar to those found in Lakkis et al. [33], although slightly higher too.

On the other hand, the distribution of vorticity per subfamily (Figure 10c) exhibits a right-skewed pattern, with most events occurring at low vorticity values between 2 and 7 $\times 10^{-5}$ 1/s. The SL systems show maximum values around 3–4 $\times 10^{-5}$ 1/s, followed by the SM subfamily with a smaller but similar pattern, while the SU subfamily shows consistently low frequencies across all values. Overall, the results indicate that low-vorticity events are much more common, while high-vorticity occurrences are relatively rare across all subfamilies. Considering trajectory length, the figure shows a clear upward trend: as distance increases, the number of events also increases, but the most notable difference between subfamilies is related to mean values: cyclones belonging to the SL subfamily travel the furthest, with an average of around 3400 km, while the SM and SU systems show values close to 2600 km and 2400 km, respectively (Figure 10d and Table 1). When combining the results shown in Figures 8 and 9 and Table 1, it appears that SL events with higher vorticity and lifetime, covering larger distances, are potentially the most reliable candidates for explaining the percentage of S2 and S3 cyclones whose genesis/lysis stage occurs above the tropopause.

Regarding the lower- and uppermost level for each family, 925 hPa, 500 hPa and 100 hPa corresponds to the lowermost level with high number of events for each family, while uppermost levels are usually mostly detected at 850 hPa, 250 hPa and 100 hPa for SL, SM and SU events, respectively (Table 2).

Table 2. Lower- and uppermost level with maximum number of events for each subfamily.

Subfamily	Lowermost Level (hPa)	Number of Events	Uppermost Level (hPa)	Number of Events
SL	925	9100	850	2282
SM	500	1825	250	1735
SU	150	717	100	924

If the lower- and uppermost levels are observed at genesis and lysis stages (Table 3), results show that shallow low systems, as expected, usually have their genesis and lysis levels mostly near the surface (925 and 850 hPa respectively). For SM cyclones, lower and upper genesis and lysis levels are observed at 500–250 hPa and 400–300 hPa, respectively. Finally, for SU systems, lower- and uppermost levels correspond to 150 and 100 hPa for genesis and 150–100 hPa for lysis phases.

Table 3. Lower- and uppermost level at genesis and lysis stage with maximum number of events in brackets for each subfamily.

Subfamily	Genesis Lowermost (hPa)	Genesis Uppermost (hPa)	Lysis Lowermost (hPa)	Lysis Uppermost (hPa)
SL	925 (6324)	850 (4063)	925 (4787)	850 (3782)
SM	500 (1128)	250 (2014)	400 (1542)	300 (1317)
SU	150 (701)	100 (682)	150 (676)	100 (659)

3.4. Basic Annual System Spatial Characteristics

Before proceeding any further and delving deeper into the average annual spatial characteristic of the systems, it is worth briefly examining some details related to the movement of the shallow cyclones. Figure 11 shows the net displacement, i.e., the path and direction of the movement, of the shallow family and subfamily events obtained as the difference between latitude and longitude of the lysis and genesis phases. As expected, the extratropical shallow systems form along and are guided by the jet stream's flow in the midlatitudes, which acts as a steering mechanism and energy source; therefore, cyclones mainly move meridionally, but they also have a significant vertical component in the displacements which becomes evident when considering the results shown above, in which the level of genesis is different to that of lysis in many cases. Similar results are obtained when subfamilies are considered. The mechanisms responsible for both horizontal and vertical movements need to be more thoroughly explained and it is beyond the scope of this analysis. However, broadly speaking, the meridional movement is supposed to be primarily driven by nonlinear advection, which can move shallow cyclones poleward but upper-level ones equatorward, while vertical movement is attributed mainly to diabatic heating and the cyclone's interaction with the background flow. A more comprehensive thesis of the different propagation mechanisms of the cyclones can be found in [41].

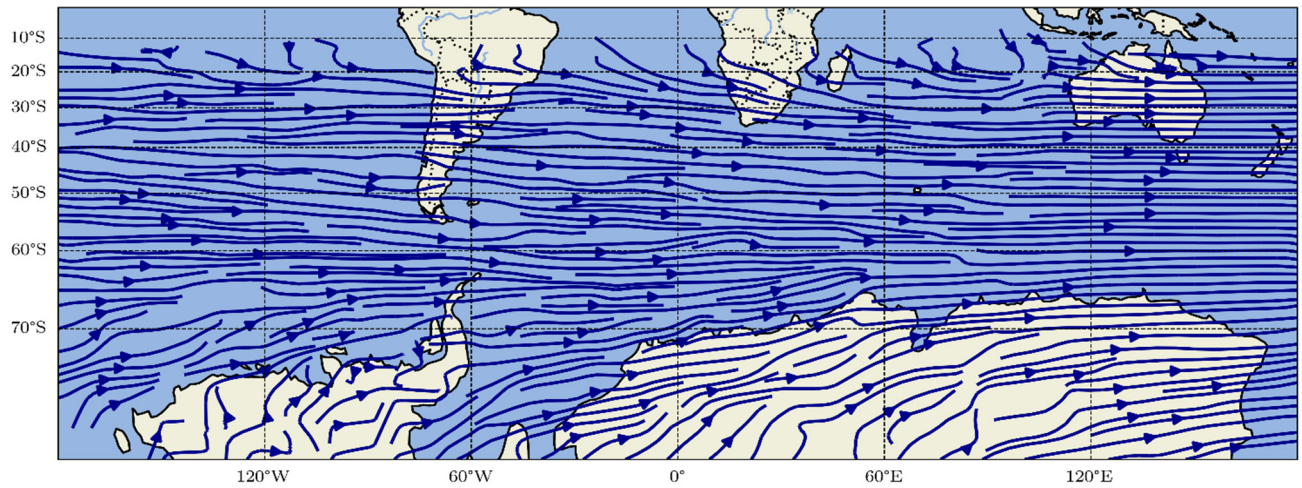

Figure 11. Net displacement of the shallow system calculated as the difference between latitude and longitude at genesis and lysis stages.

Figure 12 shows the annual spatial distribution of the cyclone density for the shallow family and subfamilies, during 2000–2023 for all multi-level systems detected. Note that this spatial density pattern complements the information provided in Figure 11; the high-density regions along the circumpolar belt correspond to the strong eastward and poleward displacement vectors visible in the net displacement field, illustrating how the preferential propagation directions of shallow cyclones translate into the observed concentration of tracks across the SH. In overall terms, the cyclones (Figure 12a) are broadly distributed from the subtropics (approx. 30° S) into the polar region, but maximum values are mainly observed in two latitudinal rings. The first extends between 30° S and 40° S, close to the subtropical jet stream, with maximum values in the Pacific Ocean and a narrow portion northwest of the Andes Mountain range, near the Altas Cumbres, between 6000 and 7000 m a.s.l., as well as in the Atlantic Ocean up to the region of southern Africa (Cape Agulhas). In the Indian Ocean, the intensity decreases, although there are some spots with very high values, especially to the north and west of Australia and near New Zealand. The second belt with high-density systems is observed in the circumpolar belt (50° S–60° S) in the vicinity of the polar jet stream, almost around the Southern Ocean, with particularly higher values off West Antarctica coast. Higher values are also observed across the Magellan Strait and the surrounding areas. Several climatological analyses of the SH have also pointed out that a high frequency of extratropical cyclones can be found in this southwestern part of the South Atlantic Ocean [13]. Lower values are observed in the belt equatorward of 20° S, except for some hotspots near the Malay Archipelago and East Timor, and also over Antarctica, approximately south of 65° S, both in the eastern and the western sector, in particular over the Weddell, Amundsen, Bellinghausen and Ross Seas and the Ronne Ice Shell. As can be seen, the distributions of the subfamilies (Figure 12b–d) show a similar pattern to the previous one throughout the hemisphere, but with decreasing density values. Minimum values can be detected in the case of SU events, where the pattern is more homogeneous and shows a minimum density value around almost all of Antarctica and in the latitudinal band between 0° S and 30° S. The observed SU density is in reasonable agreement with the subtropical cut-off low climatology obtained by [36]. In general terms, the results are consistent with those obtained by [13], although they focused mainly on seasonal results and systems observed primarily in the lower and upper troposphere. Similarities can also be found with the results shown by [31], that derived MSLP cyclones using data from the ECMWF 40-year reanalysis (ERA-40), despite differences in pressure level coverage,

tracking algorithm, and the seasonal perspective of analysis. The result is also similar to that obtained in [33], particularly in the Antarctic area.

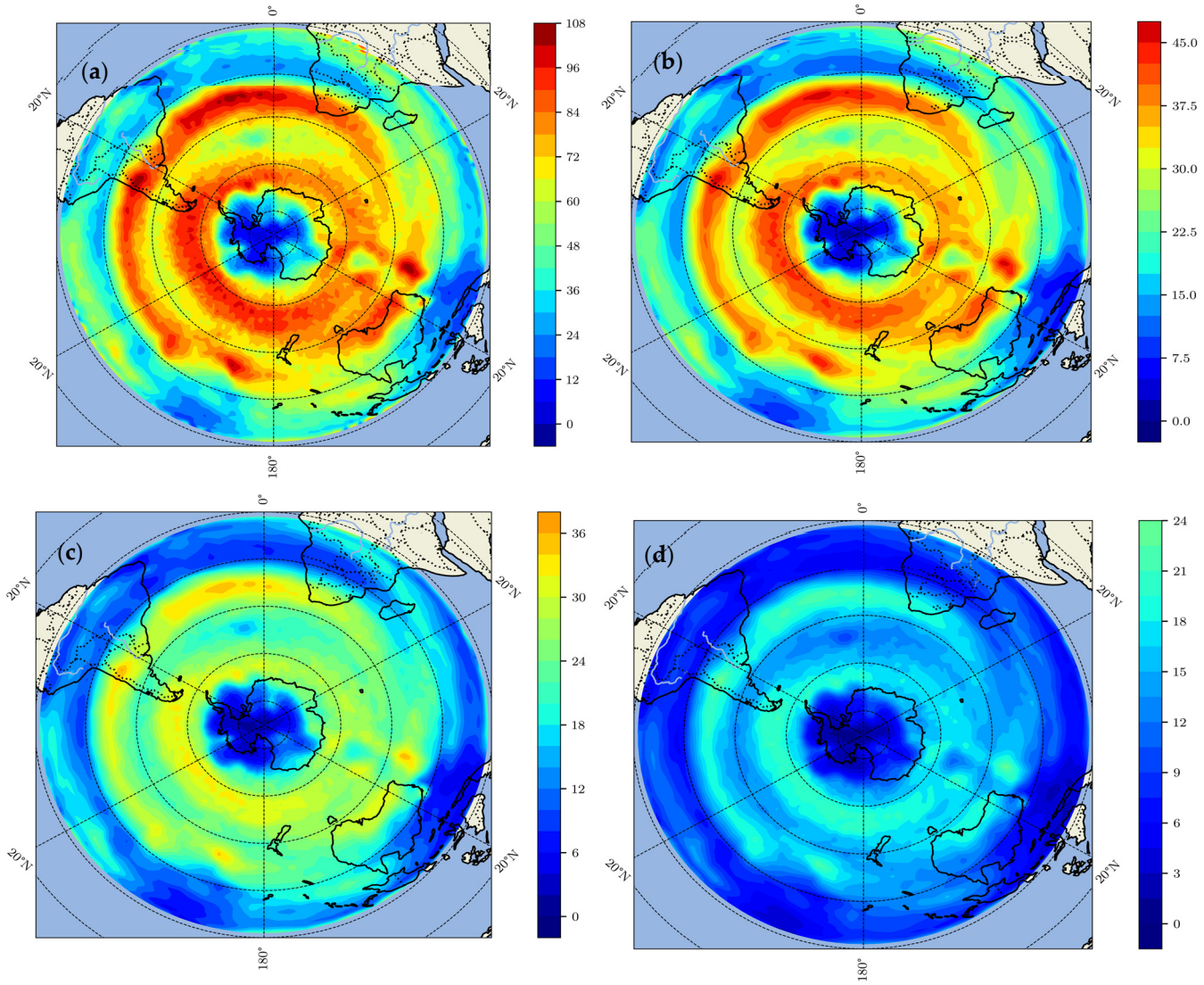

Figure 12. Annual density cyclones distribution from 2000 to 2023 for (**a**) all shallow events over SH, (**b**) shallow low, (**c**) shallow mid, and (**d**) shallow upper events. Note that different scales are used in the panels. Density is calculated as the total number of events at a given timestep where there is a track position present at each 2° × 2° pixel.

The progressive decrease in density from SL to SM to SU events, combined with the more latitudinally homogeneous pattern of SU systems, appears consistent with the distinct physical processes mentioned in Section 3.3. SL density maxima tend to coincide with regions of strong low-level baroclinicity, the subtropical jet stream belt and the polar front, where surface temperature gradients provide the primary energy source for cyclogenesis. In contrast, the more diffuse SM pattern may reflect the influence of upper-level dynamical forcing, which is less geographically constrained than surface baroclinic zones, while the SU distribution, in reasonable agreement with the subtropical cut-off low climatology of [36], suggests that these systems may respond primarily to tropopause-level dynamics rather than to surface-driven instabilities. This spatial differentiation supports the interpretation that the three subfamilies are not merely altitude-stratified subsets of a single population but likely arise from different formation mechanisms operating at different levels of the troposphere.

Genesis and lysis stages for the entire shallow family and subfamilies are shown in Figures 13 and 14, with enlarged views of selected areas provided in Supplementary Figure S1. Most cyclogenesis activity occurs between 30° S and 70° S (Figure 13a), with the highest intensities concentrated in a nearly continuous ring surrounding Antarctica over the Southern Ocean. Two primary maxima can be distinguished: one east of the Antarctic Peninsula over the Weddell Sea region and a second in the Indian Ocean sector off East Antarctica, near the Somov Sea, consistent with [57,58]. These maxima are associated with intense baroclinic zones near the Antarctic sea-ice edge and along the main SH storm tracks. The circumpolar belt is a well-documented zone of high cyclogenesis for both short-lived and long-lived midlatitude systems [1,59], where complex atmosphere–ocean–sea-ice interactions play a significant role. The relationship between sea-ice concentration over Antarctica and ETCs is complex and not yet fully understood, as correlations may vary regionally and seasonally; a detailed mechanism of these interactions exceeds the scope of this analysis, but comprehensive descriptions can be found in [60–63], among others.

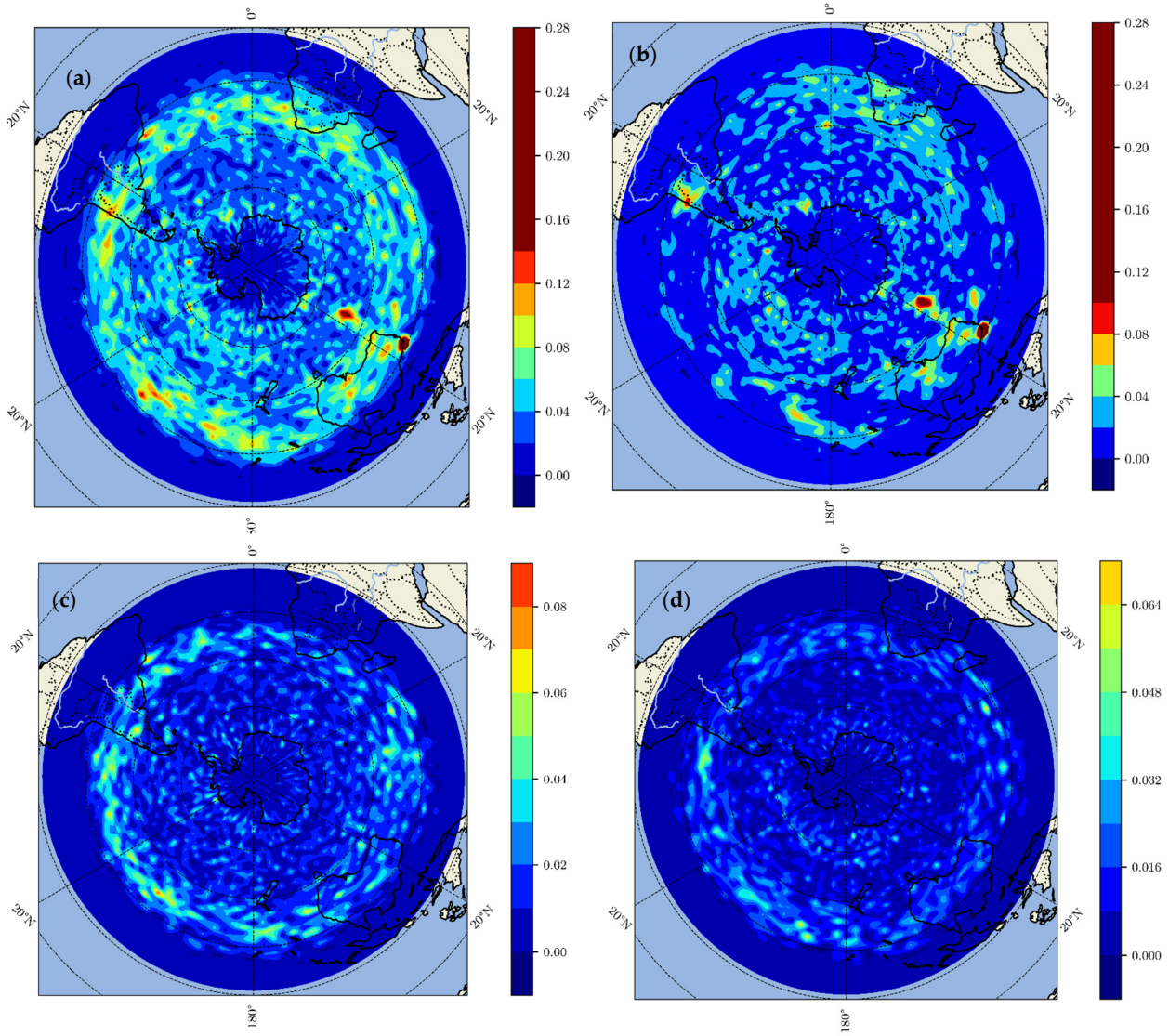

Figure 13. Genesis of (**a**) all the shallow events, (**b**) shallow low, (**c**) shallow mid, and (**d**) shallow upper events over SH for the period 2000–2023. Note that different scales are used in the panels for better viewing.

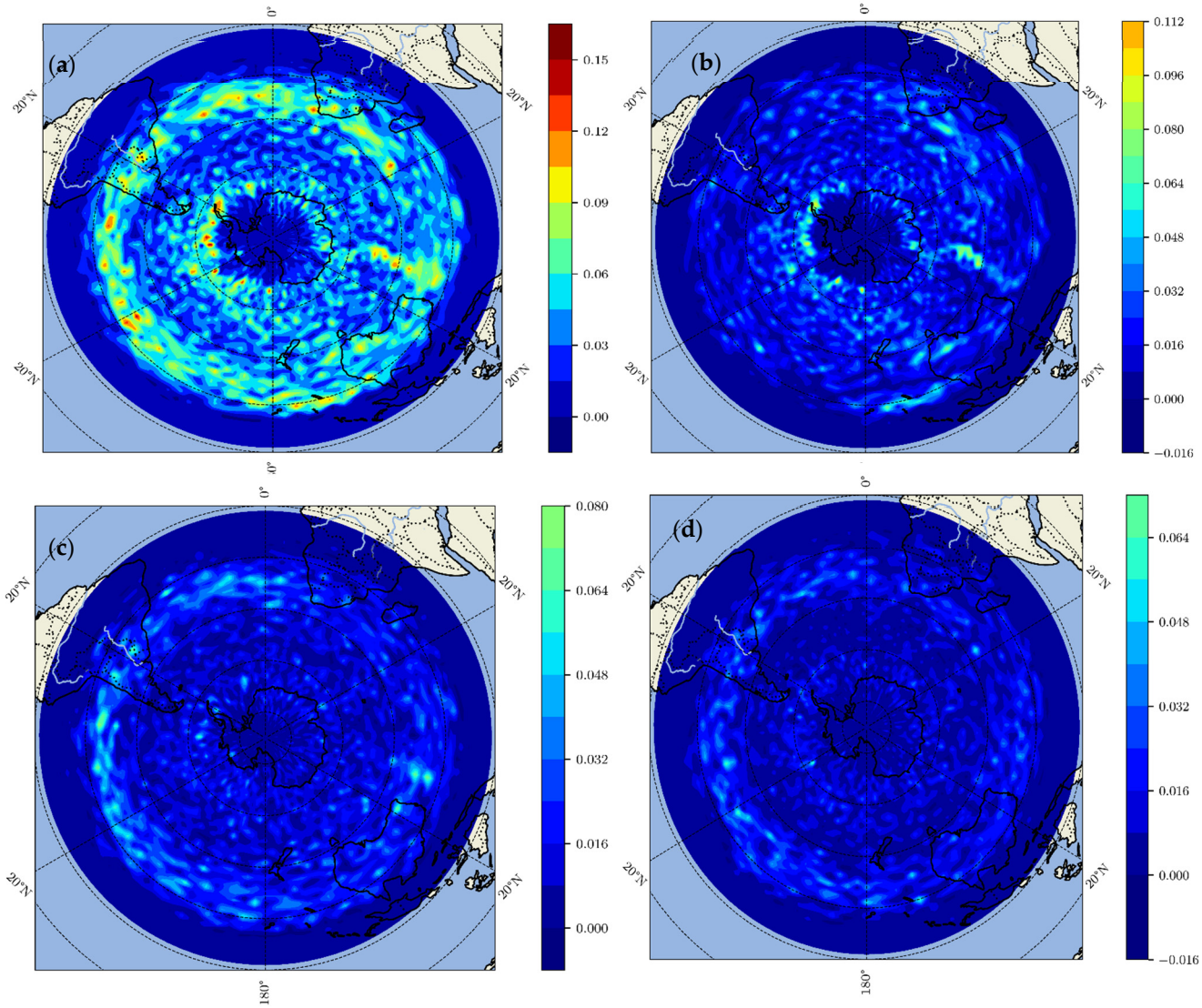

Figure 14. Lysis of (**a**) all the shallow events, (**b**) shallow low, (**c**) shallow mid, and (**d**) shallow upper events over SH for the period 2000–2023. Note that different scales are used in the panels for better viewing.

Additional cyclogenesis maxima are found off southeastern South America, adjacent to southern Brazil, Uruguay, and northern Argentina, extending southward along the Patagonian coast. This region is a well-documented area of lee-side cyclogenesis, driven by the interaction of cold polar air with subtropical moisture, Andean orographic forcing, and strong coastal SST gradients [13,28,64–66]. Lower cyclogenesis activity is observed over the western Pacific near Chile, where systems are more frequently associated with cut-off lows and upper-level PV anomalies rather than classical surface baroclinic instability [67–69].

In the African sector, cyclogenesis maxima occur over the Southwest Indian Ocean, driven by the strong baroclinic contrast between the warm Agulhas Current and cold midlatitude air masses [70], with a secondary maximum off the west coast associated with the Benguela Current and upper-level trough activity. Near New Zealand, intermediate cyclogenesis intensity is observed over the Tasman Sea and southwest of the South Island. Minimum cyclogenesis values are found in the subtropical belt equatorward of 30° S and over the Antarctic continent.

Focusing on events by subfamily, the spatial pattern (Figure 13b–d) remains fairly similar in the belt between 30° S and 45° S, but with substantial changes in intensity. For

the SL systems (Figure 13b and Supplementary Figure S1a with enlarged view of the area), areas with enhanced activity can be detected over South America, covering the region adjacent to southern Brazil, Uruguay, and Argentina (Andes Lee Cyclogenesis), primarily between 30° S and 45° S. There is also a distinct clustering of genesis events along the western and southern coasts of South Africa, especially near the Cape of Good Hope region, where the Atlantic and Indian Oceans meet and in the belt of the Southwestern Indian Ocean, south of Madagascar although with lower density. Around the Antarctic Peninsula (Supplementary Figure S1b), an intense band of high activity extends over the high southern latitudes of the Southern Ocean, particularly with higher values concentrated around the North Antarctic Peninsula and extending eastward over the Weddell Sea.

Minimum values on the other hand are observed mainly in latitudes near the Equator and the Antarctica mainland itself, where katabatic winds are dominant. With regard to SM events, the pattern is similar to that of SL events but considerably more diffuse, considering the lower densities of the events, but with the same areas of high and lower genesis. However, unlike SL events, there is a higher activity over the Antarctic Peninsula itself, particularly in the south portion of the eastern sector (Supplementary Figure S1d).

As for the lysis stages (Figure 14), the pattern for the entire family (Figure 14a) shows a distribution that resembles the genesis fields, but with a lower level of intensity and some key differences that must be noted. The highest frequency of extratropical cyclone decay is seen in a broad, nearly continuous circumpolar belt in the Southern Ocean, particularly in the very high latitudes (between 60° S and 70° S) approaching the Antarctic continent. Other areas with high intensity are found over the Weddell and Ross Sea Sectors and East Antarctica extending into the high-latitude South Indian Ocean sector. The whole area is usually known as cyclone graveyard for extratropical systems that form further north and track poleward and even for those that are generated near Antarctica which are generally found to remain near it [13]. Yuan et al. [59], in their analysis of mid-latitude cyclones in the Southern Ocean based on satellite data, highlighted the same area for the lysis stage, although with different intensities and considering both long- and short-lived systems.

The South American sector exhibits significant areas of high decay frequency over both sides of the continent, with notable concentrations near the Andes and extending into the Southwest Atlantic as part of the general high-frequency belt that merges with the circumpolar maximum further south. Over the Pacific, between 30° S and 45° S, several spots also show high decay activity, and moderate lysis frequencies occur near Australia over the Great Australian Bight and the southern continental interior.

When subfamilies are considered individually (Figure 14b–d), lysis density decreases considerably in all cases, but there are differences worth noting, especially when focusing on Supplementary Figure S1d. In South America, genesis activity exceeds lysis, consistent with the observation by Hoskins and Hodges [13] that, in the lee of the Andes, cyclogenesis is associated with the subtropical jet while system decay occurs on the upslope and regeneration on the downslope. The key role of the Andes is evident in Supplementary Figure S1a–c, where the intensity of SL lysis is higher than that of SM and SU systems, in accordance with their vertical extents. SL and, to a lesser extent, SM lysis events are concentrated along the western side of the Andes, near the Chilean coast, as observed in Lakkis et al. [33].

Regarding southern Africa, systems follow a poleward and eastward track after formation towards the Southern Ocean, with high lysis concentrated over a broad high-latitude belt south of the continent. The pattern is similar for SL, SM, and SU events, with a decrease in frequency, although SM and SU systems show greater lysis density over the continental landmass, particularly from the Cape Peninsula eastward into the

Agulhas Current region, while SU lysis appears more latitudinally homogeneous within the subtropical band.

Near Australia, all the subfamilies show high density over the entire band of the Southern Ocean surrounding Antarctica, generally poleward of °50 S. The concentration of activity around the continent highlights the role of the Circumpolar Trough acting as the preferred zone for cyclonic development and decay.

Similar to Figure 14, Figure 15 shows the family and subfamily spatial pattern, but for vorticity. For the whole family of shallow cyclones (Figure 15a) the highest overall concentration of vorticity can be observed in the main Southern Ocean storm track, a broad band that circles the continent of Antarctica, primarily between 45° S and 65° S latitude, particularly in the mid-ocean sectors over the South Indian and South Pacific Oceans. A clear local maximum in the intensity vorticity can also be found east of the Andes and extending into the South Atlantic Ocean. Although the value in this area seems slightly lower than the peak activity found in the main circumpolar storm track further south, this local maximum indicates that the cyclones formed here rapidly intensify as they move eastward off the coast. The maximum activity then moves southeast, merging into the main Southern Ocean storm track, which highlights that the South American genesis region feeds a large number of systems into the global storm track [13,71]. These areas also correspond to the regions of highest event density and also represent the vorticity maxima for SU, SM and SL events, with minimal differences in intensity (Figure 15b–d).

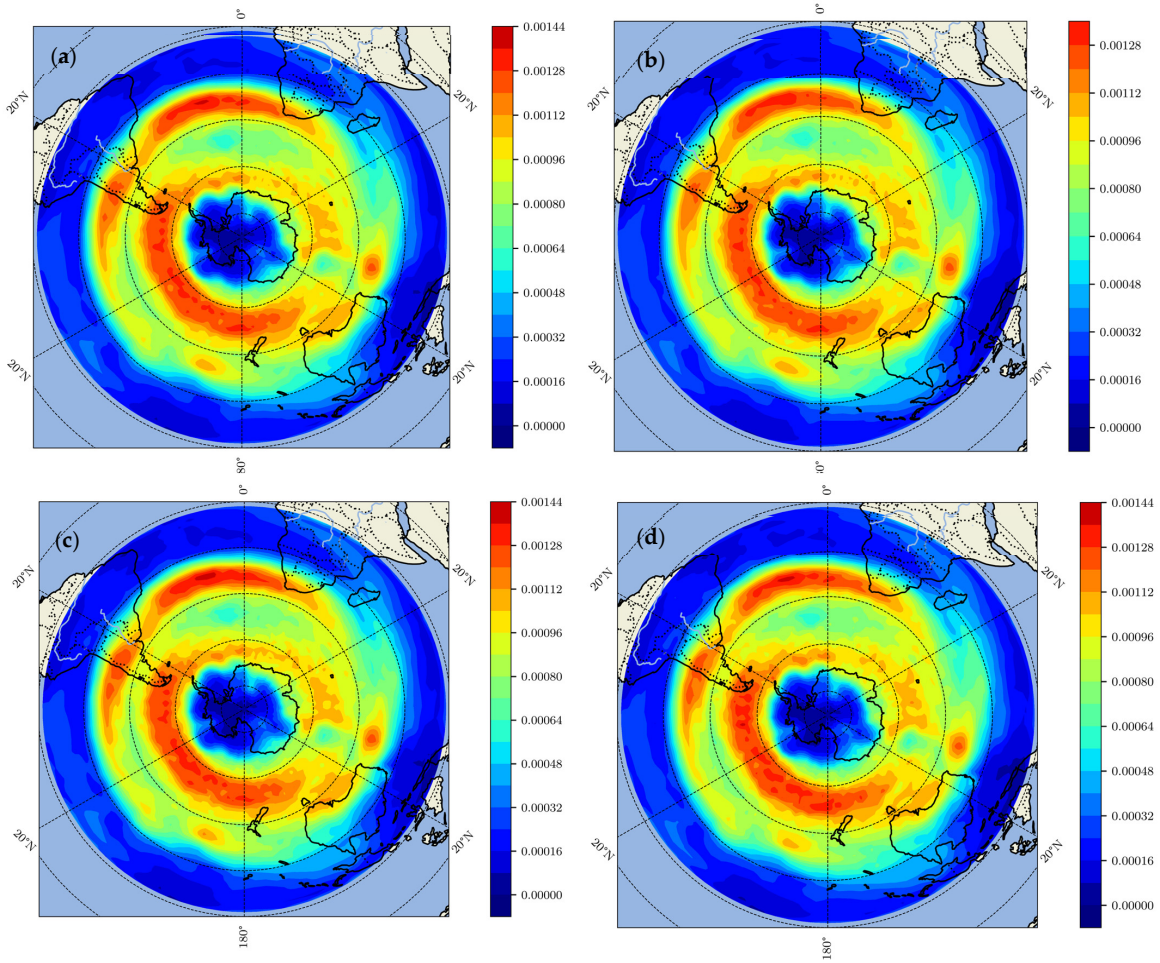

Figure 15. Vorticity × 10^{-5} (1/s) of (**a**) all the shallow events, (**b**) shallow low, (**c**) shallow mid, and (**d**) shallow upper events over SH for the period 2000–2023. Note that different scales are used in the panels.

Finally, Figure 16 shows the mean velocity for the shallow family (a) and subfamilies (b–d). As expected according to the values indicated in Table 1, the distribution for the entire family and subfamilies shows no remarkable differences in the values range. The pattern is also very similar in all cases and shows some well-defined areas with distinguishable velocity values. The first ring is over and around Antarctica with cyclones moving with velocities between 6 and 12 ms^{-1}, surrounded by a higher velocity ring between 35° S and 50° S with velocities up to 18 ms^{-1} particularly over the Pacific Ocean. This area corresponds to the location of the strongest mean westerly winds in the Southern Hemisphere. It is the tropospheric manifestation of the subtropical jet stream and the polar front jet stream, which are crucial for driving the extratropical cyclones and, according to Figure 12, this area also hosts the majority of shallows events and displays the highest vorticity values. From 30° S towards the equator, the velocity values decrease up to 6 ms^{-1}. The lowest velocities, ranging between 0 and 6 ms^{-1}, are concentrated over the polar landmass where the density and vorticity are also lower.

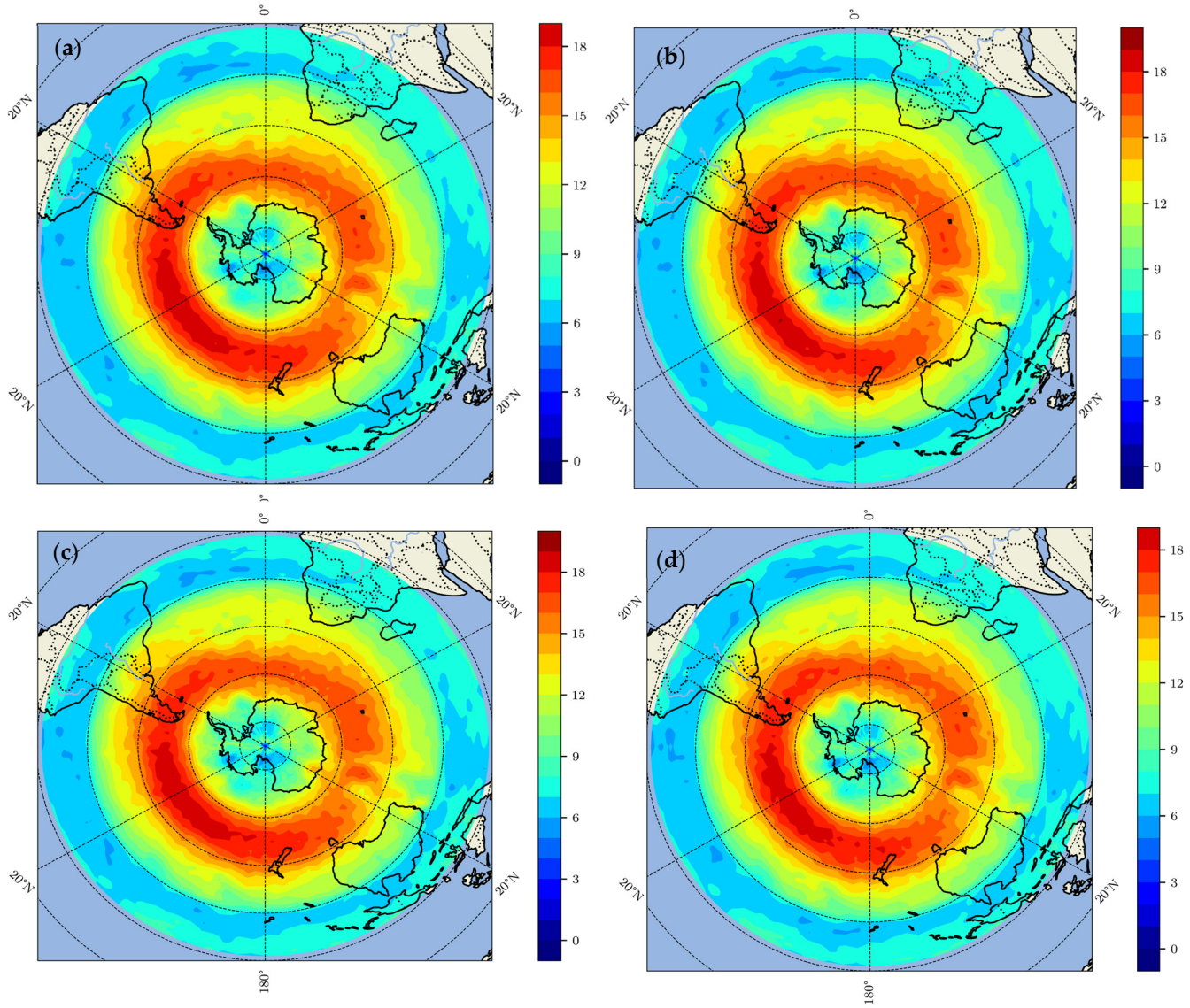

Figure 16. Velocity (m/s) of (**a**) all the shallow events, (**b**) shallow low, (**c**) shallow mid, and (**d**) shallow upper events over SH for the period 2000–2023. Note that different scales are used in the panels.

4. Discussion and Concluding Remarks

Despite the extensive body of literature on extratropical cyclones, the vast majority of existing climatologies remain confined to surface or near-surface levels, relying on single-level datasets that capture only a partial picture of these systems. The few multi-level analyses available typically span no more than six pressure levels and show significant discrepancies among themselves, leaving substantial uncertainties regarding cyclone behaviour across the full depth of the troposphere [15,31]. The present study addresses this gap by providing a comprehensive 24-year climatology of shallow extratropical cyclones across 12 pressure levels in the SH, using the STACKER multi-level tracking algorithm [32,33] and considering the cyclones as integral three-dimensional physical entities rather than isolated pressure level slices. The results show that this approach captures a substantially broader and more physically heterogeneous population of extratropical cyclones than conventional approaches, with direct implications for our understanding of midlatitude weather variability and its potential changes under a warming climate.

A total of 21,701 shallow multi-level systems were detected within the 14° S–78° S latitudinal band over the 2000–2023 period, using a minimum duration threshold of two days, accounting for 42% of all extratropical cyclones identified by the STACKER algorithm, confirming that the shallow family remains the most populous class of ETCs in the SH, consistent with [33]. The absence of a significant long-term trend, combined with the possibility of decadal to interdecadal variability, suggests that the shallow cyclone population is sensitive to low-frequency modes of climate variability rather than to the monotonic forced changes projected for deep systems [18,24]. The predominance of systems with their lowermost level near the surface (925 hPa) and their uppermost level near 125 hPa underscores the role of the tropopause as a dynamical barrier that mostly, but not always, bounds the vertical development of these systems. On average, the main characteristics of the shallow events are consistent with previous analyses [31,33]. Lower- and uppermost levels at genesis and lysis indicate that the majority of shallow systems originate and dissipate near the surface or within the mid-troposphere, although a non-negligible fraction exhibits genesis and lysis within the lower stratospheric levels.

Within the shallow cyclone population, 60% of events span two pressure levels (S2) and 40% develop across three levels (S3). Although both subtypes belong to the same family by definition, S3 systems exhibit systematically higher mean relative vorticity (~4.8×10^{-5} 1/s vs. ~4.4×10^{-5} 1/s for S2), longer lifetimes (4.46 vs. 4.13 days), and greater distances travelled (~3440 vs. ~3090 km), consistent with a more advanced stage of baroclinic coupling and stronger interaction between upper-level potential vorticity anomalies and the low-level baroclinic zone [34,35]. The distinct velocity distribution shapes, left-skewed for S2 and quasi-Gaussian for S3, further suggest that these two subtypes may arise from different large-scale forcing environments rather than representing different stages of the same developmental process [29]. Perhaps the most physically significant finding is that S3 systems exhibit a substantially higher proportion of lysis events near and above the tropopause, indicating that they are the subgroup most capable of interacting with the UTLS region, with potential consequences for stratosphere–troposphere exchange through tropopause folding and downward transport of stratospheric air [37,56]. In contrast, S2 systems, being more energetically limited and predominantly confined to the lower and middle troposphere, constitute the most frequent mode of shallow baroclinic disturbance across the SH midlatitudes.

The subfamily classification reveals that the shallow population does not represent a single class of baroclinic disturbance but rather a physically heterogeneous ensemble. The dominance of SL systems (43%) reflects the prevalence of classical surface baroclinic instability, where strong meridional temperature gradients along the polar front provide the energy

source for low-level cyclogenesis [1,34]. The substantial presence of SM events (35%) indicates that upper-level dynamical forcing, through potential vorticity anomalies propagating along the jet stream and troughs partially detached from surface baroclinicity, constitutes an independent and climatologically significant pathway for cyclone development [36]. The 22% of SU events points to a third behaviour associated with tropopause-level dynamics and cut-off lows [36,37]. Both SM and SU systems lack a detectable signature in mean sea-level pressure fields and are therefore absent from the large majority of published SH cyclone climatologies [13,28,57]. That these two subfamilies jointly account for 57% of all shallow events underscores that establishing their climatological baseline is a necessary step toward understanding how each formation regime may respond to projected changes in baroclinicity, jet stream position, and tropopause height under a warming climate [18,24].

The annual spatial density patterns show that shallow systems are distributed from the subtropics to the polar regions, with maximum density concentrated in two main latitudinal ranges: the 30° S–40° S band and the circumpolar belt (50° S–60° S), with particularly high values close to the West Antarctica sector. These results are in good agreement with [13,33]. Across subfamilies, spatial distributions remain consistent, though density values decrease progressively, reaching a minimum for SU events. The more spatially uniform distribution of SU events, compared to the geographically constrained SL pattern, is consistent with their association with upper-level dynamical processes such as Rossby wave breaking and cut-off low formation, which can occur across a broader range of latitudes wherever the jet stream undergoes sufficient meridional undulation [36,37]. This latitudinal organisation, consistent with the positions of the subtropical and polar front jet streams, confirms that shallow cyclones are steered by the same large-scale circulation features as deeper systems, while their more limited vertical development reflects a lesser degree of baroclinic energy extraction from the background flow [13,15,31].

Most cyclogenetic activity in the SH, driven primarily by land–sea distribution and baroclinic zones, occurs between 30° S and 70° S. Two primary maxima are located east of the Antarctic Peninsula, over the Weddell Sea, and within the Indian Ocean sector of the Southern Ocean. In contrast, lower cyclogenetic activity is observed over the western Pacific, near the Chilean coast, where ETCs are frequently associated with cut-off lows and potential vorticity cut-offs rather than classic surface baroclinic instability [67–69]. The fact that genesis patterns differ substantially in intensity across subfamilies, while remaining spatially similar, suggests that the three formation mechanisms share common geographic preconditioners but may respond to different dynamical triggers depending on the tropospheric level at which the instability develops.

Regarding lysis, the spatial pattern resembles the genesis fields but is displaced eastward, with the highest frequencies concentrated within a broad circumpolar belt between 60° S and 70° S. The concentration of dissipation over the high-latitude Southern Ocean suggests that the weakening of shallow cyclones is linked to the reduction in baroclinic forcing as systems move poleward into more barotropic environments [28,31]. The marked decrease in lysis density at the subfamily scale reflects the probabilistic nature of the classification: systems assigned to a subfamily based on the pressure range reached during their lifetime may dissipate at a different level, producing a more diffuse signal [33].

The mean translational velocity shows no remarkable differences across subfamilies, and the spatial patterns remain highly consistent. Distinct velocity zones are evident, with values between 6 and 12 ms^{-1} over and around Antarctica, a high-velocity ring between 35° S and 50° S reaching up to 18 ms^{-1}, and the lowest velocities over the Antarctic landmass. This spatial homogeneity indicates that the zonal propagation of shallow cyclones is governed primarily by the large-scale background flow rather than by the tropospheric

layer in which they reside. It is therefore the differences in lifetime, vorticity, and trajectory length that most clearly distinguish the dynamical character of each subgroup.

In summary, this study provides evidence-based answers to the three scientific questions posed in the Introduction. First, the degree of vertical development within the shallow family carries clear physical meaning, with S3 systems exhibiting systematically stronger dynamical properties and greater interaction with the UTLS region than S2 systems. Second, the subfamily classification confirms that the shallow population comprises three distinct classes of systems operating across different levels of the tropospheric column. Third, more than half of all shallow extratropical cyclonic activity in the SH, comprising SM and SU systems, could not be detected by conventional single-level surface-based tracking methods, reinforcing the need for 3D or 4D tracking frameworks, particularly in the context of climate projections [18,24]. The present climatology establishes a physically grounded baseline for the shallow cyclone family; subsequent analyses addressing seasonal variability and the intermediate and deep families are currently underway.

Supplementary Materials: The following supporting information can be downloaded at: https://www.mdpi.com/article/10.3390/atmos17050508/s1, Figure S1. A zoomed-in view of the areas of genesis (red dots) and lysis (blue dots) in South America and Africa (left panel) and Antarctica (right panel) for SL (a, b), SM (c, d), and SU (e, f) events.

Author Contributions: Conceptualisation, S.G.L. and P.O.C.; methodology, S.G.L., P.O.C. and G.A.F.; validation, S.G.L., P.O.C., G.A.F. and A.E.Y.; formal analysis, S.G.L.,G.A.F. and P.O.C.; investigation, S.G.L.; resources, S.G.L. and P.O.C.; data curation, G.A.F., P.O.C. and S.G.L.; writing—original draft preparation, S.G.L.; writing—review and editing, S.G.L., P.O.C., G.A.F. and A.E.Y.; visualisation, S.G.L., P.O.C., G.A.F. and A.E.Y.; supervision, S.G.L., P.O.C., G.A.F. and A.E.Y.; project administration, S.G.L. and P.O.C.; funding acquisition, S.G.L., P.O.C. and A.E.Y. All authors have read and agreed to the published version of the manuscript.

Funding: This research was funded by Universidad Tecnológica Nacional, Facultad Regional Buenos Aires, Argentina, grants number MSTCBA0008661 and MSTCBA0008639.

Institutional Review Board Statement: Not applicable.

Informed Consent Statement: Not applicable.

Data Availability Statement: The ERA5 reanalysis data used in this study are publicly available from the Copernicus Climate Data Store (CDS) at https://cds.climate.copernicus.eu/ (accessed on 15 June 2025).

Acknowledgments: The authors would like to thank CONICET and Pontificia Universidad Católica Argentina.

Conflicts of Interest: The authors declare no conflicts of interest.

References

1. Ulbrich, U.; Leckebusch, G.C.; Pinto, J.G. Extra-tropical cyclones in the present and future climate: A review. *Theor. Appl. Climatol.* **2009**, *96*, 117–131. [CrossRef]
2. Browning, K.A. The sting at the end of the tail: Damaging winds associated with extratropical cyclones. *Q. J. R. Meteorol. Soc.* **2004**, *130*, 375–399. [CrossRef]
3. Catto, J.L.; Jakob, C.; Berry, G.; Nicholls, N. Relating global precipitation to atmospheric fronts. *Geophys. Res. Lett.* **2012**, *39*, L10805. [CrossRef]
4. Sinclair, V.; Rantanen, M.; Haapanala, P.; Räisänen, J.; Järvinen, H. The characteristics and structure of extratropical cyclones in a warmer climate. *Weather Clim. Dyn.* **2020**, *1*, 1–25.
5. Chen, T.-C.; Di Luca, A. Characteristics of Precipitation and Wind Extremes Induced by Extratropical Cyclones in Northeastern North America. *J. Geophys. Res. Atmos.* **2025**, *130*, e2024JD042079. [CrossRef]

6. IPCC. Contribution of Working Group I to the Fourth Assessment Report. In *Climate Change 2007: The Physical Science Basis*; Solomon, S., Qin, D., Manning, M., Marquis, M., Averyt, K., Tignor, M.M.B., Miller, H.L., Chen, Z., Eds.; Cambridge University Press: Cambridge, UK, 2007.
7. IPCC. Contribution of Working Groups I, II and III to the Fifth Assessment Report. In *Climate Change 2014: Synthesis Report*; Pachauri, R.K., Meyer, L.A., Eds.; IPCC: Geneva, Switzerland, 2014.
8. Valsangkar, A.A.; Monteiro, J.M.; Narayanan, V.; Hotz, I.; Natarajan, V. An exploratory framework for cyclone identification and tracking. *IEEE Trans. Vis. Comput. Graph.* **2019**, *25*, 1460–1473. [CrossRef]
9. Bjerknes, J. On the Structure of Moving Cyclones. *Geofys. Publ.* **1919**, *1*, 95. [CrossRef]
10. Picornell, M.; Jansà, A.; Genovés, A.; Campins, J. Automated database of mesocyclones from the HIRLAM(INM)-0.5 analyses in the western Mediterranean. *Int. J. Climatol.* **2001**, *21*, 335–354. [CrossRef]
11. Jansa, A.; Genoves, A.; Picornell, M.; Campins, J.; Riosalido, R.; Carretero, O. Western Mediterranean cyclones and heavy rain. Part 2: Statistical approach. *Meteorol. Appl.* **2001**, *8*, 43–56. [CrossRef]
12. Hanson, C.; Palutikof, J.; Davies, T. Objective cyclone climatologies of the North Atlantic—A comparison between the ECMWF and NCEP Reanalyses. *Clim. Dyn.* **2004**, *22*, 757–769. [CrossRef]
13. Hoskins, B.J.; Hodges, K.I. A new perspective on southern hemisphere storm tracks. *J. Clim.* **2005**, *18*, 4108–4129. [CrossRef]
14. Kouroutzoglou, J.; Flocas, H.A.; Keay, K.; Simmonds, I.; Hatzaki, M. On the vertical structure of Mediterranean explosive cyclones. *Theor. Appl. Climatol.* **2012**, *110*, 155–176. [CrossRef]
15. Pepler, A.; Dowdy, A. A three-dimensional perspective on extratropical cyclone impacts. *J. Clim.* **2020**, *33*, 5635–5649. [CrossRef]
16. Walker, E.; Mitchell, D.; Seviour, W. The numerous approaches to tracking extratropical cyclones and the challenges they present. *Weather* **2020**, *75*, 336–341. [CrossRef]
17. Geng, Q.; Sugi, M. Possible Change of Extratropical Cyclone Activity due to Enhanced Greenhouse Gases and Sulfate Aerosols—Study with a High-Resolution AGCM. *J. Clim.* **2003**, *16*, 2262–2274. [CrossRef]
18. Bengtsson, L.; Hodges, K.I.; Roeckner, E. Storm tracks and climate change. *J. Clim.* **2006**, *19*, 3518–3543. [CrossRef]
19. Catto, J.L.; Shaffrey, L.C.; Hodges, K.I. Northern Hemisphere Extratropical Cyclones in a Warming Climate in the HiGEM High-Resolution Climate Model. *J. Clim.* **2011**, *24*, 5336–5352. [CrossRef]
20. Mizuta, R. Future Change in Extratropical Cyclones Associated with the Interdecadal Pacific Oscillation. *J. Clim.* **2011**, *24*, 6505–6521.
21. Chang, E.K.M.; Guo, Y.; Xia, X. CMIP5 multimodel ensemble projection of storm track change under global warming. *J. Geophys. Res.* **2012**, *117*, D23118. [CrossRef]
22. Zappa, G.; Shaffrey, L.C.; Hodges, K.I. The ability of CMIP5 models to simulate north Atlantic extratropical cyclones. *J. Clim.* **2013**, *26*, 5379–5396. [CrossRef]
23. Michaelis, A.C.; Willison, J.; Lackmann, G.M.; Robinson, W.A. Changes in Winter North Atlantic Extratropical Cyclones in High-Resolution Regional Pseudo–Global Warming Simulations. *J. Clim.* **2017**, *30*, 6905–6925. [CrossRef]
24. Priestley, M.D.K.; Catto, J.L. Future changes in the extratropical storm tracks and cyclone intensity, wind speed, and structure. *Weather. Clim. Dyn.* **2022**, *3*, 337–360. [CrossRef]
25. Colle, B.A.; Zhang, Z.; Lombardo, K.A.; Chang, E.; Liu, P.; Zhang, M. Historical Evaluation and Future Prediction of Eastern North American and Western Atlantic Extratropical Cyclones in the CMIP5 Models during the Cool Season. *J. Clim.* **2013**, *26*, 6882–6903. [CrossRef]
26. Grieger, J.; Leckebusch, G.C.; Donat, M.G.; Schuster, M.; Ulbrich, U. Southern Hemisphere winter cyclone activity under recent and future climate conditions in multimodel AOGCM simulations. *Int. J. Climatol.* **2014**, *34*, 3400–3416. [CrossRef]
27. Pfahl, S.; O'Gorman, P.A.; Singh, M.S. Extratropical cyclones in idealized simulations of changed climates. *J. Clim.* **2015**, *28*, 9373–9392. [CrossRef]
28. Simmonds, I.; Keay, K. Variability of Southern Hemisphere Extratropical Cyclone Behavior, 1958–1997. *J. Clim.* **2000**, *13*, 550–561. [CrossRef]
29. Neu, U.; Akperov, M.G.; Bellenbaum, N.; Benestad, R.; Blender, R.; Caballero, R.; Cocozza, A.; Dacre, H.F.; Feng, Y.; Fraedrich, K.; et al. IMILAST: A community effort to intercompare extratropical cyclone detection and tracking algorithms. *Bull. Am. Meteorol. Soc.* **2013**, *94*, 529–547. [CrossRef]
30. Di Luca, A.; Evans, J.P.; Pepler, A.S.; Alexander, L.; Argüeso, D. Resolution sensitivity of cyclone climatology over eastern Australia using six reanalysis products. *J. Clim.* **2015**, *28*, 9530–9549. [CrossRef]
31. Lim, E.; Simmonds, I. Southern hemisphere winter extratropical cyclone characteristics and vertical organization observed with the ERA-40 data in 1979–2001. *J. Clim.* **2007**, *20*, 2675–2690. [CrossRef]
32. Lakkis, S.; Canziani, P.; Yuchechen, A.; Rocamora, L.; Caferri, A.; Hodges, K.; O'Neill, A. A 4D feature-tracking algorithm: A multidimensional view of cyclone systems. *Q. J. R. Meteorol. Soc.* **2019**, *145*, 395–417. [CrossRef]
33. Lakkis, S.G.; Canziani, P.O.; Rodriguez, J.O.; Yuchechen, A.E.; O'NEill, A.; Albers, K.H.; Hodges, K. Early 21st Century cyclone climatology: A 3D perspective. Basic Characterization. *Int. J. Climatol.* **2021**, *41*, 4019–4046. [CrossRef]

34. Hoskins, B.J.; McIntyre, M.E.; Robertson, A.W. On the use and significance of isentropic potential vorticity maps. *Q. J. R. Meteorol. Soc.* **1985**, *111*, 877–946. [CrossRef]
35. Holton, J.R.; Hakim, G.J. *An Introduction to Dynamic Meteorology*, 5th ed.; Academic Press: Waltham, MA, USA, 2013; 532p.
36. Pinheiro, H.R.; Hodges, K.I.; Gan, M.A.; Ferreira, N.A. A new perspective of the climatological features of upper-level cut-off lows in the Southern Hemisphere. *Clim. Dyn.* **2017**, *48*, 541–559. [CrossRef]
37. Škerlak, B.; Sprenger, M.; Wernli, H. A global climatology of stratosphere–troposphere exchange using the ERA-Interim data set from 1979 to 2013. *Atmos. Chem. Phys.* **2014**, *14*, 913–937. [CrossRef]
38. Hersbach, H.; Bell, B.; Berrisford, P.; Hirahara, S.; Horányi, A.; Muñoz-Sabater, J.; Nicolas, J.; Peubey, C.; Radu, R.; Schepers, D.; et al. The ERA5 global reanalysis. *Q. J. R. Meteorol. Soc.* **2020**, *146*, 1999–2049. [CrossRef]
39. Hodges, K.I. Feature tracking on the unit-sphere. *Mon. Weather Rev.* **1995**, *123*, 3458–3465. [CrossRef]
40. Hodges, K.I. Adaptive constraints for feature tracking. *Mon. Weather Rev.* **1999**, *127*, 1362–1373. [CrossRef]
41. Yao, Y.; Zhang, Y.; Hodges, K.I.; Tamarin-Brodsky, T. Different Propagation Mechanisms of Deep and Shallow Wintertime Extratropical Cyclones over the North Pacific. *J. Clim.* **2023**, *36*, 8277–8297. [CrossRef]
42. Kendall, M.G. A New Measure of Rank Correlation. *Biometrika* **1938**, *30*, 81–93. [CrossRef]
43. Hoffmann, L.; Günther, G.; Li, D.; Stein, O.; Wu, X.; Griessbach, S.; Heng, Y.; Konopka, P.; Müller, R.; Vogel, B.; et al. From ERA-Interim to ERA5: The considerable impact of ECMWF's next-generation reanalysis on Lagrangian transport simulations. *Atmos. Chem. Phys.* **2019**, *19*, 3097–3124. [CrossRef]
44. McErlich, C.; McDonald, A.; Renwick, J.; Schuddeboom, A. An Assessment of Southern Hemisphere Extratropical Cyclones in ERA5 Using WindSat. *J. Geophys. Res. Atmos.* **2023**, *128*, e2023JD038554. [CrossRef]
45. Marrafon, V.H.; Reboita, M.S.; da Rocha, R.P.; Crespo, N.M. Ciclones extratropicais no hemisfério sul: Comparação entre diferentes reanálises. *Rev. Bras. Climatol.* **2021**, *28*, 48–73. [CrossRef]
46. Bischoff, S.; Canziani, P.O.; Yuchechen, A.E. The tropopause at southern extratropical latitudes: Argentine operational rawinsonde climatology. *Int. J. Climatol.* **2007**, *27*, 189–209. [CrossRef]
47. Hoffmann, L.; Spang, R. An assessment of tropopause characteristics of the ERA5 and ERA-Interim meteorological reanalyses. *Atmos. Chem. Phys.* **2022**, *22*, 4019–4046. [CrossRef]
48. Hirschberg, P.A.; Fritsch, J.M. Tropopause undulations and the development of extratropical cyclones. Part I: Overview and observations from a cyclone event. *Mon. Weather Rev.* **1991**, *119*, 496–517. [CrossRef]
49. Qian, S.; Hu, H.; Hodges, K.I.; Yang, X.-Q.; Song, T. Synergistic forcing of the troposphere and stratosphere on explosively developing cyclones over the North Pacific during cold season. *Geophys. Res. Lett.* **2024**, *51*, e2024GL110069. [CrossRef]
50. Canziani, P.O.; Legnani, W.E. Tropospheric–stratospheric coupling: Extratropical synoptic systems in the lower stratosphere. *Q. J. R. Meteorol. Soc.* **2003**, *129*, 2315–2329. [CrossRef]
51. Nathan, T.R.; Hodyss, D. Troposphere–stratosphere communication through local vertical waveguides. *Q. J. R. Meteorol. Soc.* **2010**, *136*, 12–19. [CrossRef]
52. Seiler, C.; Zwiers, F.W. How will climate change affect explosive cyclones in the extratropics of the Northern Hemisphere? *Clim. Dyn.* **2016**, *46*, 3633–3644. [CrossRef]
53. Seiler, C.; Zwiers, F.W. How well do CMIP5 climate models reproduce explosive cyclones in the extratropics of the Northern Hemisphere? *Clim. Dyn.* **2016**, *46*, 1241–1256. [CrossRef]
54. Seiler, C. A Climatological Assessment of Intense Extratropical Cyclones from the Potential Vorticity Perspective. *J. Clim.* **2019**, *32*, 2369–2380. [CrossRef]
55. Palmen, E.; Newton, C.W. *Atmospheric Circulation Systems*; Academic Press: New York, NY, USA, 1969; pp. 471–522.
56. Sprenger, M.; Croci Maspoli, M.; Wernli, H. Tropopause folds and cross-tropopause exchange: A global investigation based upon ECMWF analyses. *J. Geophys. Res. Atmos.* **2003**, *108*, 8518.
57. Wernli, H.; Schwierz, C. Surface cyclones in the ERA-40 dataset (1958–2001). Part I: Novel identification method and global climatology. *J. Atmos. Sci.* **2006**, *63*, 2486–2507. [CrossRef]
58. de Souza, M.R.; Piva, E.D. Storm tracks and cyclogenesis over the Southern Ocean: An overview with the HadGEM3-GC3.1 model. *Int. J. Climatol.* **2023**, *43*, 7565–7587. [CrossRef]
59. Yuan, X.; Patoux, J.; Li, C. Satellite-based midlatitude cyclone statistics over the Southern Ocean: 2. Tracks and surface fluxes. *J. Geophys. Res. Atmos.* **2009**, *114*, D04106. [CrossRef]
60. Vichi, M.; Eayrs, C.; Alberello, A.; Bekker, A.; Bennetts, L.; Holland, D.; de Jong, E.; Joubert, W.; MacHutchon, K.; Messori, G.; et al. Effects of an explosive polar cyclone crossing the Antarctic marginal ice zone. *Geophys. Res. Lett.* **2019**, *46*, 5948–5958. [CrossRef]
61. Uotila, P.; Vihma, T.; Pezza, A.B.; Simmonds, I.; Keay, K.; Lynch, A.H. Relationships between Antarctic cyclones and surface conditions as derived from high-resolution numerical weather prediction data. *J. Geophys. Res.* **2011**, *116*, D07109. [CrossRef]
62. Ward, J.L.; Payne, A.E.; Pettersen, C. Present-day regional Antarctic Sea Ice response to extratropical cyclones. *J. Geophys. Res. Atmos.* **2023**, *128*, e2023JD038914. [CrossRef]

63. Zhong, R.; Hodges, K.; Yang, Q.; Chen, D. Revisiting the interaction between Antarctic sea ice and Southern Ocean cyclones. *J. Geophys. Res. Atmos.* **2025**, *130*, e2024JD042914. [CrossRef]
64. Mendes, D.; Souza, E.P.; Marengo, J.A.; Mendes, M.C.D. Climatology of extratropical cyclones over the South American–southern oceans sector. *Theor. Appl. Climatol.* **2009**, *98*, 239–250. [CrossRef]
65. Dalanhese, L.; Stuivenvolt-Allen, J.; LaPlante, M.; Wang, S.; Costa, T.L.; da Silva, H.D.F.; Belem, A.L. A new climatology of South American extratropical cyclogenesis with an intercomparison among ERA5, JRA55 and the Brazilian Navy. *Int. J. Climatol.* **2023**, *43*, 7050–7066. [CrossRef]
66. Gramcianinov, C.B.; Hodges, K.I.; Camargo, R. Early-Stage Extratropical Cyclones' Mechanisms Over South America: RCM Added Value and Future Changes in a Warmer Planet. *Int. J. Climatol.* **2025**, *45*, e8683. [CrossRef]
67. Gómez-Contreras, Á.; Carrera-Ávila, N.; Rapanague, M.J.; Rondanelli-Rojas, R. Cutoff Lows, Moisture Plumes, and Their Influence on Extreme-Precipitation Days in Central Chile. *J. Appl. Meteorol. Climatol.* **2021**, *60*, 437–457.
68. Crespo, N.M.; Reboita, M.S.; Rocha, R.P. The role of potential vorticity on the development of a subtropical cyclone over the South Atlantic Ocean. *Clim. Resil. Sustain.* **2022**, *1*, e15.
69. Reboita, M.S.; da Rocha, R.P.; Crespo, N.M. Extratropical cyclone activity over the South Atlantic Ocean: A review of the current knowledge and future perspectives. *Int. J. Climatol.* **2018**, *38*, 2866–2879. [CrossRef]
70. Reason, C.J.C. Evidence for the Influence of the Agulhas Current on Regional Atmospheric Circulation Patterns. *J. Clim.* **2001**, *14*, 2769–2778. [CrossRef]
71. Vera, C.S.; Vigliarolo, P.K.; Berbery, E.H. Cold Season Synoptic-Scale Waves over Subtropical South America. *Mon. Weather. Rev.* **2002**, *130*, 684–699. [CrossRef]